Received: 25 November 2021 | Revised: 23 January 2022 | Accepted: 11 February 2022

DOI: 10.1002/ese3.1101

ORIGINAL ARTICLE

Comprehensive thermoeconomic, exergoeconomic, and optimization analyses of direct oxy-combustion supercritical CO_2 intercooled and reheated cycles under design and off-design conditions

Wahib A. Al-Ammari | **Ahmad K. Sleiti**

Department of Mechanical and Industrial Engineering, College of Engineering, Qatar University, Doha, Qatar

Correspondence
Wahib A. Al-Ammari and Ahmad K. Sleiti, Department of Mechanical and Industrial Engineering, College of Engineering, Qatar University, Zone no. 65, Street no. 875, P.O. Box. 2713, Doha 122104, Qatar.
Email: wahib.alammari@qu.edu.qa and asleiti@qu.edu.qa

Funding information
Qatar National Research Fund, Grant/Award Number: NPRP-S grant # [11S-1231-170155]

Abstract

This study presents comprehensive energetic, exergetic, exergoeconomic, and economic (4E) performance analyses for four direct oxy-combustion (DOC) supercritical carbon dioxide (sCO_2) power cycles at design, off-design, and part-load conditions. These cycles include the dual recuperator cycle (DRC), intercooling cycle (ICC), partial intercooling cycle (PIC), and reheating cycle (RHC). The analyses were conducted at relatively low turbine inlet temperatures (TIT: 550–750°C) with compressor inlet temperature (CIT) varied from 33°C (wet-cooling) to 50°C (dry-cooling). Furthermore, single- and multiobjective optimization analyses were conducted for each cycle. At design conditions (high-pressure of $P_{c,o} = 20$ MPa, low-pressure of $P_{c,o} = 5.4$ MPa, TIT = 750°C, CIT = 50°C [dry-cooling]), the PIC has the highest thermal efficiency (47.78%) compared to 38.36% for DRC, 45.71% for ICC, and 44.39% for RHC. At optimized conditions ($P_{c,o} = 30$ MPa, $P_{c,o} = 8$ MPa, TIT = 744°C, CIT = 30°C [wet-cooling]), the ICC shows superior energetic performance (52.08%) compared to 47.97% for DRC, 49.20% for PIC, and 48.62% for RHC. At off-design conditions with a power demand (PD) of 40% of the design load (50 MW), the thermal efficiency is decreased by 21.82% in DRC, 17.71% in ICC, 22.46% in PIC, and 13.60% in RHC. The ICC has the minimum levelized cost of electricity compared to the other cycles with 5.93 ¢/kWh at design conditions (dry-cooling), 5.65 ¢/kWh at optimized conditions (wet-cooling), and 7.2 ¢/kWh at minimum PD (21 MW). Therefore, from an economic point of view, the ICC is recommended as the best power block for a sCO_2 power cycle driven by oxy-combustor at moderate TITs. The study also provides constructive comparisons between the DOC-sCO_2 and indirect (nuclear, solar, and waste heat) sCO_2 power cycle systems and the future research directions.

KEYWORDS
4E analysis, design and off-design performance, direct oxy-combustion, multiobjective optimization, part-load operation, supercritical CO_2 power cycles, wet and dry cooling

1 | INTRODUCTION

In the recent decade, the worldwide interest in the supercritical carbon dioxide (sCO_2) power cycles has been increased steadily.[1] This returns to the distinguishing features of the sCO_2 power cycles, such as compactness,[2] high efficiencies,[3] and ability to capture CO_2 emissions.[4] These sCO_2 power cycles can be integrated with a variety of applications, such as[5]: (1) nuclear reactors (which were reviewed in Wu et al.[6] and analyzed in Du et al.[7]); (2) concentrated solar power (CSP), which were reviewed in Li et al.,[8] presented for dry-cooling conditions in Khatoon et al.,[9] and introduced with direct integration as in Son et al.,[10] or indirect integration as in Linares et al.[11]; (3) waste heat recovery through integration with bottoming cycles,[12] direct carbon fuel cell,[13] coupling with high-grade waste heat sources,[14] or specific industries such as steel industry,[15] and direct oxy-combustion (DOC) technologies.[16] Therefore, in the open literature, various configurations for the sCO_2 power block are proposed and investigated for these applications. The major proposed configurations were simple recuperator cycle (SRC), dual recuperator cycle (DRC), intercooling cycle (ICC), partial intercooling cycle (PIC), reheating cycle (RHC), recompression cycle (RCC), precompression cycle (PCC), and preheating cycle (PHC).[17] Some of these configurations were thermodynamically and economically assessed and compared for the aforementioned applications with a focus on the CSP technologies[18] and waste heat recovery.[19] The RCC was recommended as the most efficient and economical configuration with an efficiency higher than 50% at heat source temperatures less than 800°C as designed by Saeed et al.,[20] analyzed by Khatoon et al.,[21] and optimized by Milani et al.[22] However, some of these configurations are not applicable for DOC technologies such as RCC for the reasons mentioned in Sleiti and Al-Ammari.[23] Furthermore, there is a lack of comprehensive comparison between the feasible configurations for the DOC technology based on thermodynamic and economic performance indicators. Moreover, these configurations were not compared at their optimized and off-deign conditions. Thus, the present study is presented to fulfill these gaps, see Figure 1. The next four paragraphs introduce a comprehensive review of the most relevant studies to the present work.

The DOC technologies are mainly developed to generate electricity at high efficiency by capturing CO_2 emissions. Over the past few decades, several DOC-based power cycles have been proposed such as the Graze cycle,[24] MATIANT (contraction of the names of the two designers MAThieu and lANTovski) cycle,[25] the semi-closed oxy-combustion combined cycle (SCOC-CC),[26] and Allam cycle.[16] Currently, the Allam cycle is one of the most promising direct oxy-fuel power cycles, which can capture 98.9% of the combustion products with an energy efficiency of 58.9%[27] for natural gas and 51.44% for gasified coal.[1] However, the design of the Allam cycle's components is quite challenging and costly as it operates at very high pressure (300 bar) and temperature (1150°C).[28] In particular, the regenerator has to handle five cold and hot streams, including turbine exhaust flow, recycled sCO_2 flow, oxidant, turbine coolant flow, and flow that transfers heat from the air separation unit (ASU) to the regenerator to correct the thermodynamic imbalance that occurs in the regenerator. This imposed an extremely large heat transfer area and robust structure to withstand the pressure differences (200–300 bar) and

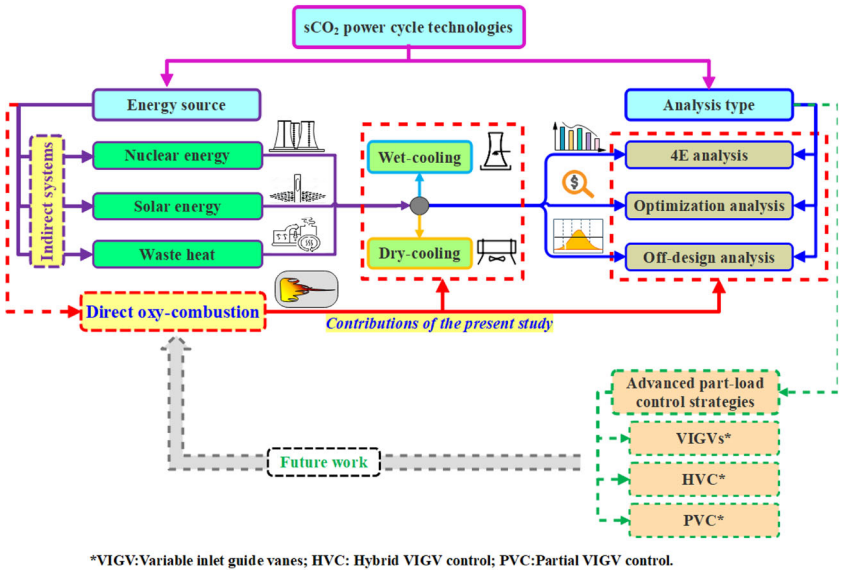

FIGURE 1 The main contributions of the current study: 4E, optimization, off design, wet- and dry-cooling

high temperatures (700–750°C).[29] Recently, several studies attempted to introduce some modifications and applications for the Allam cycle to further enhance its efficiency and minimize its operational costs. For instance, Liu et al.[30] proposed chemical looping combustion instead of conventional combustion in the Allam cycle, which could improve its electricity efficiency by 9.5%. Other studies adapted the Allam cycle for polygeneration coal-based[31] or biomass-based[32] systems, integrated it with regasification of liquid natural gas,[19] or Haber-Bosch process.[33] However, these processes still suffer from complexity and high capital investment. Therefore, improving the performance of the Allam cycle or similar DOC cycles should be initialized first by selecting the suitable configuration and operating conditions of the power block to make facilitate their commercialization.

The performance of several sCO_2 power cycles at design conditions was investigated based on energetic, exergetic, exergoeconomic, and economic (4E) analyses by several research groups. For instance, Rogalev et al.[34] proposed construction for a high-power sCO_2 gas turbine based on a thermodynamic study with a specific investment of 1307.5 $/kW, which is 46% lower than that of a combined cycle power plant (2424 $/kW). Li et al.[19] showed that integrating the Allam cycle with regasification of liquified natural gas improves the energy efficiency by 16% over the conventional Allam cycle. However, the exergy efficiency did not exceed 52%, which is lower than those reported for sCO_2 power cycles driven by nuclear (67.28%[35]) or solar energy (78%[36]) and similar to sCO_2 power cycles driven by waste energy (52.73%[37]). This implies that cycles with moderate energy source temperatures (550–750°C) have higher exergy efficiencies than Allam-based cycles. Further, 4E analyses were conducted on integrated cooling-heating-power (CHP) systems where the sCO_2 power block is integrated as a top[38] or bottoming cycle[39] with a focus on freshwater production,[40] hydrogen generation,[41] refrigeration cycle,[42] and waste heat recovery.[43] However, compared to the benefits of these systems, their complexity makes them less attractive for practical applications as their economic feasibility was not confirmed in most of these studies. Only a two 4E analysis studies for DOC-based sCO_2 cycles at moderate turbine inlet temperatures (TITs) were introduced in open literature. One with particular focus on the preheating process as designed in Sleiti et al.[29] and the other one with optimization analysis at dry and wet cooling conditions as conducted in Sleiti et al.[44] However, a comprehensive comparison of different DOC-based sCO_2 cycles is still needed to point out the most feasible and economic configuration, which is performed for the first time in the present study.

While the 4E analyses are useful tools that provide guidelines for preliminary design of the cycle components and give clear insights to which configuration has more potential to be used, they cannot tell the best energetic and economic operating scenarios. This is mainly because of the trade-offs between the operating conditions that yield the highest energetic performance and those that yield a minimum levelized cost of electricity (LCOE). Thus, optimization analysis is necessary to address these trade-offs. Techno-economic optimized analysis of nine sCO_2 power cycles driven by CSP was introduced by Thanganadar et al.[45] They concluded that a recompression cycle with intercooling can reduce the overnight capital cost by 10.8% compared to the basic recompression cycle at TIT of 700°C. But their analysis is limited to the capital cost without reporting the LCOE for these configurations. However, the LCOE for CSP-based Allam and partial cooling sCO_2 power cycles are estimated to be in the range from 8 to 11 ¢/kWh as reported by Crespi et al.[46] In the open literature, only three studies[29,47,48] reported the LCOE for DOC-based sCO_2 power cycles working at TIT between 550 and 750°C. However, these studies are limited to preheating (6.3 ¢/kWh)[47] and flared-power cycles (7.7 ¢/kWh).[48] Therefore, further economic analysis for DOC-based cycles is needed to assess the economic feasibility of various configurations other than preheated and flared cycles, which is one of the major contributions of the present study as shown in Figure 1.

In addition to the 4E and optimization analyses of the sCO_2 power cycle, the off-design analysis is a fundamental step to improve its performance by maintaining stable operation using proper control strategies. Dyreby et al.[49–51] have developed modeling methodology to predict the steady-state performance of sCO_2 power cycles at off-design and design conditions. This methodology was used by many researchers to analyze the off-design performance of several sCO_2 power cycles, such as CSP-based,[52] waste heat-based,[19] nuclear-based,[53] and coal-based[54] cycles. For the Allam cycle, Zaryab et al.[55] introduced a detailed part-load model to evaluate the off-design performance maps of its compressors, pumps, and turbine. They recommended optimizing the adjustment of compressors' guide vanes and the minimum cycle pressure to achieve higher efficiency at part-load operation. Also, Scaccabarozzi et al.[56] performed part-load analysis for the Allam cycle without considering the ASU into account. They mentioned that as the power load decreases from 100% to 40%, the decrease in the normalized efficiency of the Allam cycle is about 3% lower than that of a combined power cycle. However, only one study in open literature investigated the off-design performance of a DOC-based cycle integrated with CSP by Sleiti and Al-Ammari.[57] As such, the current study

introduces a thorough analysis of stand-alone DOC-based sCO_2 power cycles at off-design conditions.

Sleiti and Al-Ammari[23] have performed energetic and exergetic performance analyses for five DOC sCO_2 power cycles, including SRC, DRC, ICC, PIC, and RHC. These analyses were performed at turbine inlet temperatures of (TIT: 550–750°C), compressor inlet temperatures of (CIT: 32–50°C), maximum pressure of ($P_{c,o} = 20$ MPa), and pressure ratio of (r_c: 2–5). They found that the SRC has the lowest energy and exergy efficiencies (34.44% and 79.70%, respectively), PIC achieved the highest thermal efficiency (47.57%), while the highest exergy efficiency of 88.10% is achieved by the RHC. However, merely energy and exergy analyses are not sufficient to decide which cycle is the best fit for the DOC-sCO_2 technology. This is because of the considerable difference in the configuration of each cycle which may negatively affect their economic feasibility. So, further economic analyses are needed to point out which cycle is more feasible from an economic point of view. Furthermore, Sleiti and Al-Ammari[23] concluded that there is a trade-off between the conditions of the optimum energy and exergy efficiency, thus an optimization analysis must be conducted. Moreover, to have a more accurate and comprehensive comparison, these configurations should be investigated and compared at off-design and part-load operation conditions. Therefore, as shown in Figure 1, this study comprehensively addresses these gaps by implementing comprehensive economic, optimization, and off-design analysis for these cycles except the SRC. The SRC is not considered for further analyses due to its poor energetic and exergetic performances. Based on the above and referring to Figure 1, the main contributions of the current study are:

(1) Performing comprehensive energetic, exergetic, exergoeconomic, and economic (4E) analyses for four DOC-sCO_2 power cycles, including DRC, ICC, PIC, and RHC. Although several 4E studies in open literature have been conducted on indirect sCO_2 power cycles, this is the first 4E analysis for direct oxy-combustion sCO_2 power cycles.
(2) Finding the optimal operating conditions of these cycles using both single- and multiobjective optimization analyses.
(3) Investigating the off-design performance (including the part-load operation) for each cycle under an arid climate and for various PD scenarios.
(4) Comparing the performance indicators (efficiencies, total product unit cost, and LCOE) of these cycles with other common sCO_2 cycles applied for nuclear reactors and concentrated solar power technologies.

The rest of the article is organized into four more sections as follows: Section 2 describes the operating mechanisms and technical features of the investigated cycles. Section 3 presents the energetic, exergetic, exergoeconomic, economic (4E), and off-design models developed for the analyses of these cycles. Section 4 introduces and discusses the obtained results in three main sections, including the design analysis results (Section 4.1), optimization results (Section 4.2), and off-design analysis results (Section 4.3). Finally, the conclusions and future work suggestions of this study are presented in Section 5.

2 | DESCRIPTION OF THE INVESTIGATED DIRECT OXY-COMBUSTION SUPERCRITICAL CO_2 CYCLES

The layouts and *T–s* diagrams of the investigated cycles in this study are presented in Figure 2. The layout of the DRC (Figure 2A) is used as a reference configuration to explain the operating mechanism of each system. High-purified oxygen is supplied to the oxy-combustor (State 11) using an ASU to be directly combusted with natural gas (assumed as pure methane, State 10). Then, the CO_2 and water vapor (combustion products) enter the turbine (State 1) at high pressure (20–30 bar) and moderate temperatures (550–750°C) and expanded to the low-pressure side (Process 1–2). Next, the turbine outlet flow undergoes the processes from State 2 to 3 and from 3 to 4 in both the high-temperature recuperator (HTR) and low-temperature recuperator (LTR) to preheat the high-pressure recycled CO_2 flow. Then, the low-pressure flow is cooled down in the precooler (PC, Process 4–5) and water vapor is condensed and separated via the waster separator (WS, Process 5–6). At State 6, CO_2 flow is compressed to the desired high-pressure (State 7). At State 7, part of the compressed CO_2 is exported to be used in commercial applications or sequestrated.[58] The other part is recycled (referred to as rCO_2) to the combustor to mitigate the temperature of the oxy-combustion products after being preheated in the LTR (7–8) and HTR (8–9). The rCO_2 is then mixed with pressurized oxygen (State 10) and fuel (State 11) and combusted in the combustor to repeat the cycle (see *T–s* diagram of the DRC in Figure 2A).

In ICC (Figure 2B), the compression process of the CO_2 flow is performed in two stages (6–7 and 8–9) with an intercooling process through the intercooler (IC) to minimize the compression power. In PIC (Figure 2C), only a fraction of the rCO_2 flow undergoes the intercooling process (7–8) and the other fraction is

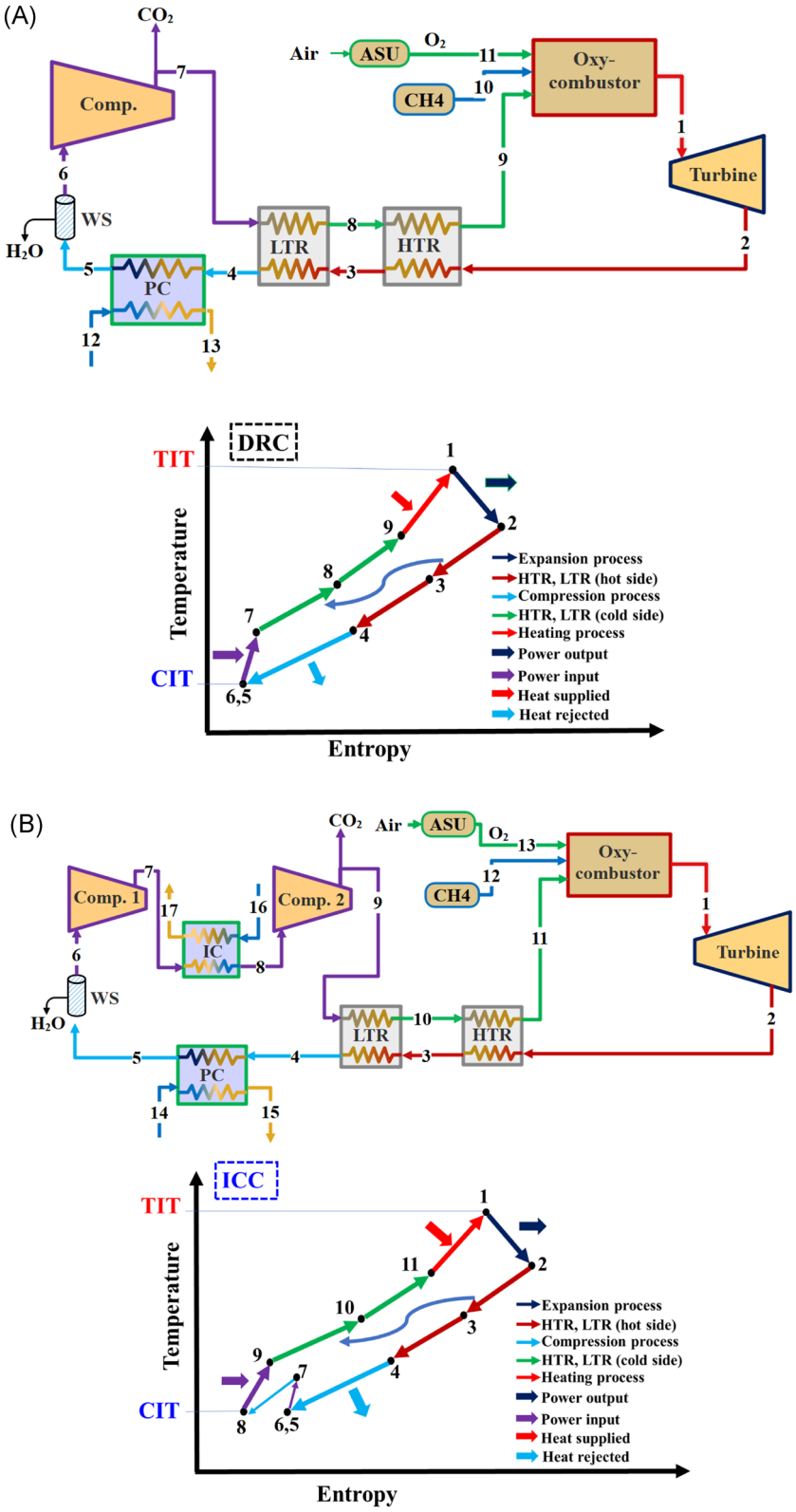

FIGURE 2 Layouts and *T–s* diagrams of the (A) dual recuperator cycle (DRC), (B) intercooling cycle (ICC), (C) partial intercooling cycle (PIC), and (D) reheating cycle (RHC). ASU, air separation unit; CIT, compressor inlet temperature; TIT, turbine inlet temperature

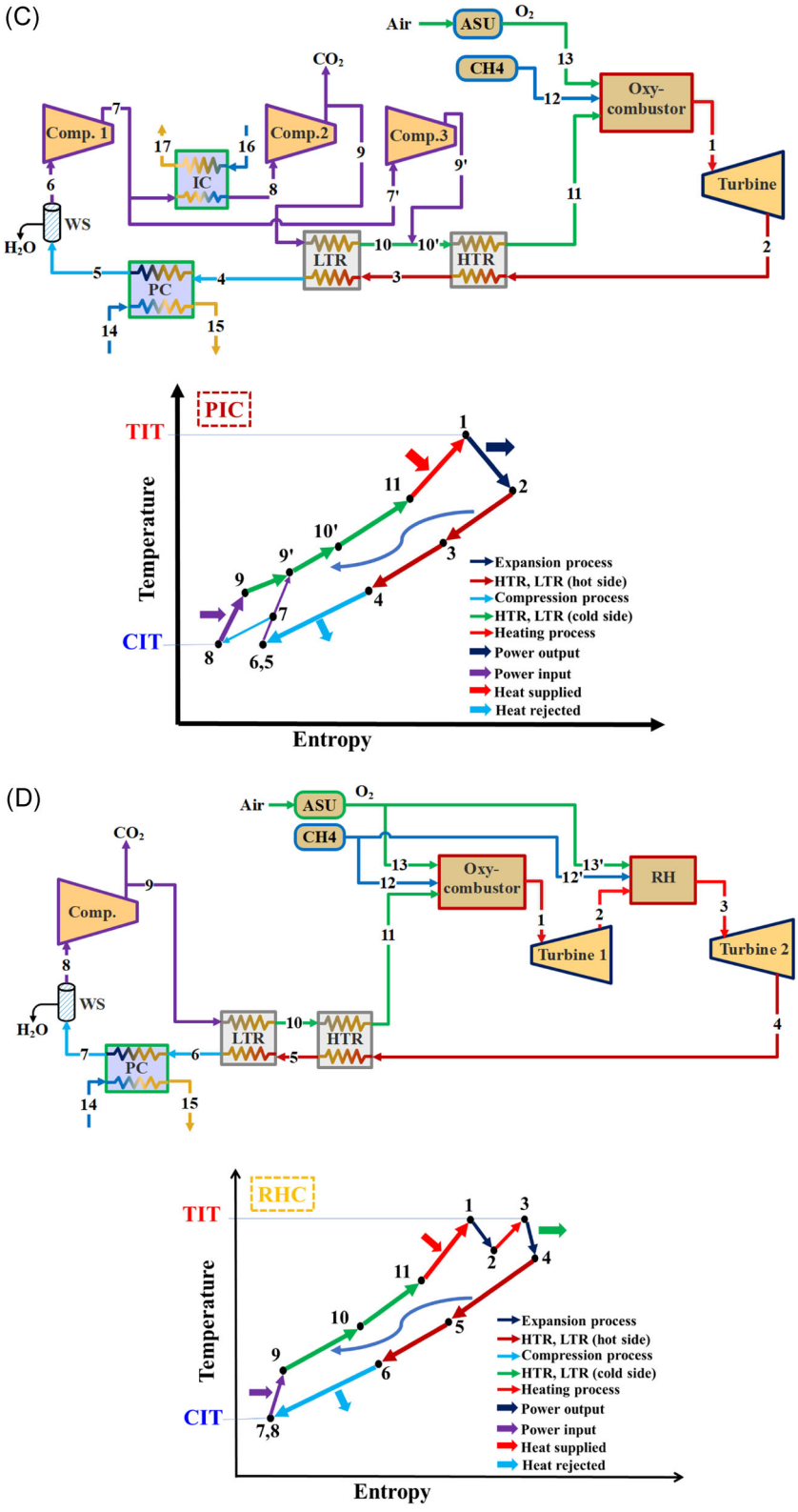

FIGURE 2 Continued

compressed (7′–9′) and mixed with the previous fraction at the exit of the LTR (State 10′). In RHC (Figure 2D), the expansion process is carried out in two stages through Turbine 1 (1–2) and Turbine 2 (3–4) with a reheating process (2–3) by another oxy-combustor, referred to as reheater (RH).

Compared to the DRC, the main feature of the ICC is that minimized compression power is achieved by applying the intercooling process. For nuclear reactors and solar power technologies, the recompression sCO_2 cycle is recommended as the most efficient configuration as only a fraction of the rCO_2 passes through the LTR, which attenuates its pinch point problem.[1] For the DOC technology, this technique can be only performed by the PIC. Thus, PIC minimizes the compression power and also enhances the performance of the LTR, which makes its energetic performance superior. In addition, the RHC is able to produce larger output power compared to the other cycles.[59] However, the addition of other compressors, IC, RH, and/or turbine to the basic layout of the DRC makes their economic feasibility and off-design control quite challenging.[60] For a fair comparison between these configurations, these configurations must be compared under the same design and off-design conditions. To do that, 4E models must be developed and validated first, as presented in the next section.

3 | MATHEMATICAL MODEL

This section describes the 4E models that were developed for the analysis of the investigated DOC-sCO_2 power cycles. Throughout the analysis, a steady-state operation is assumed, and kinetic and potential energies variations are neglected.

3.1 | Thermodynamic models

The energy and exergy models of each cycle were developed by applying the mass and energy conservation principles of each component, such that:[23,61]

$$\sum \dot{m}_i = \sum \dot{m}_o, \tag{1}$$

$$\sum \dot{Q} + \sum \dot{m}_i h_i = \sum \dot{W} + \sum \dot{m}_o h_o, \tag{2}$$

$$\dot{E}_Q + \sum \dot{E}_i = \dot{E}_W + \sum \dot{E}_o + \dot{E}_D. \tag{3}$$

Furthermore, the thermodynamic model of the LTR, HTR, IC, and PC was based on the effectiveness method using Equation (4)[23,62] where variable specific heat of the CO_2 as a function of temperature is taken into consideration as detailed in Sleiti and colleagues.[23,29]

$$\in = \frac{\dot{Q}}{\dot{Q}_{\max}}. \tag{4}$$

The thermal efficiency for each cycle is expressed as the ratio of the net output power ($\dot{W}_{\text{net}}$) to the total input power ($\dot{Q}_{\text{in}}$) as:

$$\eta_{\text{th}} = \frac{\dot{W}_{\text{net}}}{\dot{Q}_{\text{in}}}, \tag{5}$$

where the equations of $\dot{W}_{\text{net}}$ and $\dot{Q}_{\text{in}}$ are given in the Supporting Information Material (Table S1).

For the exergy model, the physical and chemical exergies are given as[23,63]:

$$\dot{E}_{\text{ph}} = \dot{m}((h - h_o) - T_o(s - s_o)), \tag{6}$$

$$\dot{E}_{\text{ch}} = \dot{n}\left[\sum_{j=1}^{n} x_j e_j^o + RT_o \sum_{j=1}^{n} x_j \ln\,(x_j)\right], \tag{7}$$

where $\dot{n}$ is the molar flow rate, x_j is the molar fraction of jth component in a mixture, and e_j^o is the standard chemical exergy of jth component at T_o and P_o conditions. To evaluate the exergy efficiency of each cycle, the fuel-product-loss method is used. For kth component, the balanced equation of fuel-product-loss exergies and exergy efficiency are expressed as in Equations (8) and (9), respectively.[64,65] The fuel and product exergies for each component of the present cycles are defined in the Supporting Information Material (Table S2).[59]

$$\dot{E}_{D,k} = \dot{E}_{F,k} - \dot{E}_{P,k} - \dot{E}_{L,k}, \tag{8}$$

$$\varepsilon_k = \frac{\dot{E}_{P,k}}{\dot{E}_{F,k}}. \tag{9}$$

The overall exergy efficiency of each system is:

$$\varepsilon_{\text{overall}} = \frac{\sum \dot{E}_{P,k}}{\sum \dot{E}_{F,k}}. \tag{10}$$

3.2 | Exergoeconomic and economic models

The product cost per unit exergy is obtained by the exergoeconomic model of each cycle. It is initiated by applying the cost balance equation to each component to obtain the cost rate of each stream, which is given as follows:

$$\sum \dot{C}_{\text{out},k} + \dot{C}_{\text{po},k} = \sum \dot{C}_{\text{in},k} + \dot{C}_{q,k} + \dot{Z}_k, \quad (11)$$

where $\dot{C}_{\text{in},k}$, and $\dot{C}_{\text{out},k}$ are inlet and outlet cost rates of each stream. $\dot{C}_{q,k}$ and $\dot{C}_{\text{po},k}$ are the cost rates of the thermal energy input and power output of each component (if existed). $\dot{Z}_k$ represents the sum of capital investment, maintenance, and operating costs, which is expressed as in Equation (23).[66]

$$\dot{Z}_k = \left(\frac{\text{CRF}}{\tau}\right) Z_k + \gamma_k Z_k/\tau, \quad (12)$$

where the capital cost of each component (Z_k) is presented in the Supporting Information Material (Table S3). The plant operation time (τ) per year is taken as (7446 h), while the weighting coefficient (γ_k) is fixed at 0.06. The CRF is the capital recovery factor, which is related to the interest rate ($\omega = 12\%$) and the lifetime of the plant ($n = 20$ years):

$$\text{CRF} = \frac{\omega \cdot (1+\omega)^n}{(1+\omega)^n - 1}. \quad (13)$$

The total product unit cost ($c_{P,\text{total}}$) is calculated as follows:

$$c_{P,\text{total}} = \frac{\sum_{i=1}^{n_k} \dot{Z}_k + \sum_{i=1}^{n_f} c_f \dot{E}_F}{\sum_{i=1}^{n_p} \dot{E}_P}. \quad (14)$$

For the present cycles, the cost balance equations are presented in the Supporting Information Material (Table S4). The economic assessment of the present cycles is presented in terms of the LCOE[67]:

$$\text{LCOE} = \frac{\text{PC} - \text{PV}_{\text{DTS}} + \text{PV}_{\text{LOC}} - \text{PV}_{\text{SC}}}{\text{LEP}}, \quad (15)$$

where the project cost (PC) is the sum of the components and installation costs (given in Equation 16), the depreciation tax shield present value (PV_{DTS}), lifetime operation costs (PV_{LOC}) are expressed in Equations (17) and (18), respectively. The present value of salvage costs (PV_{SC}) is assumed to be \$0.00, while the lifetime electrical production (LEP) is given in Equation (19).

$$\text{PC} = \sum(\text{Component cost} + \text{Installation cost})_k, \quad (16)$$

$$\text{PV}_{\text{DTS}} = \text{TR} \times \text{PC}/(1+\text{DR})^{\text{DP}}, \quad (17)$$

$$\text{PV}_{\text{LOC}} = n * (\text{OMC} + \text{Cost of the fuel})/(1+\text{DR})^n, \quad (18)$$

$$\text{LEP} = \text{PUF} \times n \times \dot{W}_{\text{net}} \times 8760. \quad (19)$$

The design values of the parameters presented in Equations (16)–(19) are also presented in Table 1. Also, the capital cost functions of each component are presented in the Supporting Information Material (Table S3). Furthermore, the direct labor and installation costs were taken as 12% of the capital component cost.[70]

TABLE 1 Parameters at the design point

Parameter	Unit	Range/ design value
Design output power, P_{net}	MW	50
Turbine inlet temperature, $T_{t,i}$	°C	550–750/750
Inlet temperature of compressor, $T_{t,i}$	°C	33–50/50
Ambient air temperature, T_o	°C	35
Compressor outlet pressure, $P_{c,o}$	MPa	20–30/20
Pressure ratio, $r_c = P_{c,o}/P_{c,i}$		2–6/3.67
Intermediate pressure ratio, $\text{RPR} = [(P_{c,o}/P_{\text{im}}) - 1]/[r_c - 1]$		0.43
Ambient pressure, P_o	kPa	101.33
Turbine isentropic efficiency, η_t[68]	%	93
Compressor isentropic efficiency, η_c[68]	%	89
LHV (methane)	kg/kJ	50,050
Specific power consumption of ASU, SPC_{ASU}	kW/kgO_2	900
Combustor pressure drops[69]	%	3
Recuperator pressure drops (hot side)[28]	%	3
Recuperator pressure drops (cold side)[69]	%	1
Precooler, intercooler, and water separator pressure drops[28]	%	2
Lifetime of the plant, n	years	20
Period of depreciation, PD	years	10
Tax rate, TR	%	35
Interest rate, ω	%	12
Plant utilization factor, PUF	%	85
Operating and maintenance cost	$\$/\text{kWh}_e$	0.008
Fuel cost	$\$/\text{kWh}_e$	0.07
Turbine diameter, D_t	m	0.60
Compressor diameter, D_c	m	0.48
Shaft speed, $N_{c,\text{design}}$	rpm	13,000

3.3 | Off-design model

The off-design analyses of the present cycles were performed based on the off-design methodology developed by Dyreby et al.[50] using sCO_2 experimental data from Sandia National Laboratory.[50] In this method, the modified flow coefficient (ϕ^*), ideal head coefficient (ψ^*), and efficiency (η^*) are given by Equations (20), (21), and (22), respectively.

$$\phi^* = \frac{\dot{m}_{CO_2}}{\rho U_c D_c^2}\left(\frac{N}{N_{design}}\right)^{1/5}, \tag{20}$$

$$\psi^* = \frac{\Delta h_i}{U_c^2}\left(\frac{N_{design}}{N}\right)^{(20\phi^*)^3}, \tag{21}$$

$$\eta^* = \eta\left(\frac{N_{design}}{N}\right)^{(20\phi^*)^5}, \tag{22}$$

where ρ and $\dot{m}$ are the density and mass flow rate at the compressor inlet, respectively. N_{design}, N, D_c, and U_c are the design shaft speed, operational shaft speed, rotor diameter, and rotor tip speed, respectively. Δh_i represents the ideal enthalpy rise in the compressor. Across the turbine, the mass flow rate is given by Equation (23) asfollows:

$$\dot{m}_{CO_2} = C_s A_{nozzle} \rho_{out}, \tag{23}$$

where C_s is called the spouting velocity, which is the velocity that could be achieved if the fluid is isentropically expanded through an ideal nozzle). A_{nozzle} is the effective nozzle area, and ρ_{in} is the fluid density at the turbine outlet.

To obtain the isentropic efficiency at the off-design conditions ($\eta_{t,off}$), first, the ideal aerodynamic efficiency is obtained as:

$$\eta_{aero,ideal} = 2\nu\sqrt{1-\nu^2}, \tag{24}$$

where ν is the ratio of the turbine tip to spouting velocities:

$$\nu = \frac{U_t}{C_s}, \tag{25}$$

$$C_s = \sqrt{2\,\Delta h_i}. \tag{26}$$

Then, $\eta_{aero,ideal}$ is substituted to obtain $\eta_{t,off}$:

$$\eta_{t,off} = \eta_{design}\eta_{aero,ideal}. \tag{27}$$

Finally, under the off-design conditions, the model of the recuperators is given as follows:

$$\frac{UA_{off}}{UA_{design}} = \left(\frac{\dot{m}_{CO_2,off}}{\dot{m}_{CO_2,design}}\right)^{0.8}. \tag{28}$$

3.4 | Solution procedures

As shown in Figure 3, the solution of the developed models is carried out in three major steps, including (1) solution of the 4E models at design condition, (2) solution of the single- and multioptimization models (discussed in Section 4.2), and (3) solution of the off-design model based on the optimized results of Step (2). 4E models were solved based on the design conditions presented in Table 1, which are carefully selected to match the practical ranges recommended for DOC-sCO_2 power cycles.[23] The solution was conducted using the real thermodynamic properties of all fluids available in the library of the Engineering Equation Solver platform. For part-load operation, the PD profile and the ambient conditions were obtained using scaled data for the maximum PD day (September 7) and minimum PD day (February 1) in Qatar.[57,71,72]

3.5 | Model validation

The developed model for each cycle was validated by comparing the energy analysis results with similar cycles used in other technologies under the same operating conditions as provided in Table 2. The results show a good agreement with a maximum error in the thermal efficiency of 1.83% and a minimum error of 0.71%. The error source may be owed to several reasons, such as the accuracy of the HTR and LTR models used in the references (discretized vs. nondiscretized approach, number of segments, etc.); the source of the thermodynamic properties for each study; and the assumptions made for the analysis.

To validate the off-design analysis model, a comparison was made between the published results by Dyreby et al.[51] and the present model for the DRC under the same conditions (Figure 4). As the off-design model solution depends on the iterative process for the adjustment of the rotor speed and compressor inlet pressure, the error varies over the range of the CIT and TIT. However, the maximum ARE does not exceed 2.1% (only for a limited number of points), while the average ARE is only 1.15% for CIT and 1.35% for TIT.

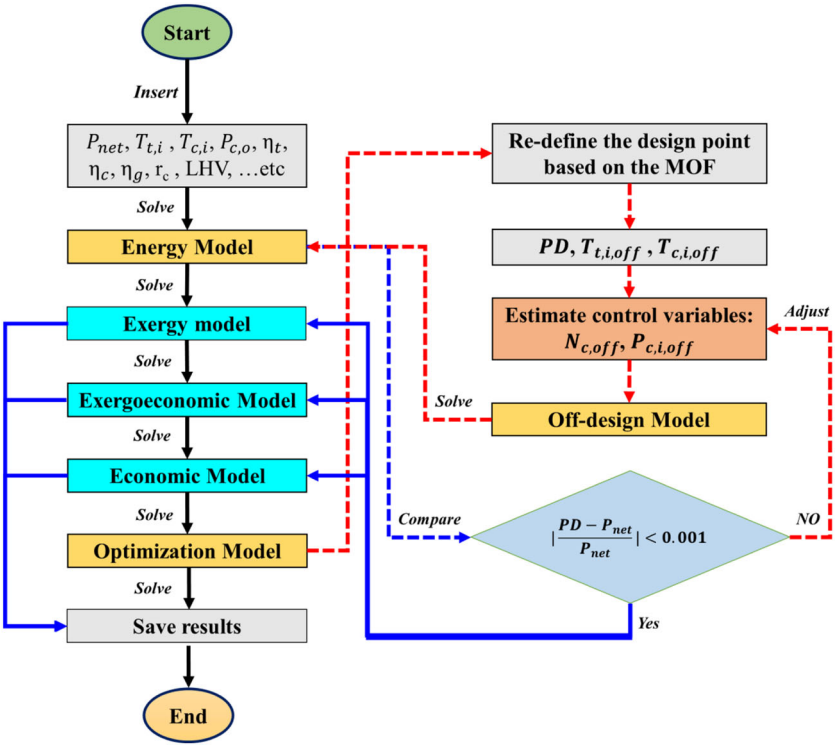

FIGURE 3 Solution procedures of the 4E, optimization, and off-design models. MOF, multiobjective function

4 | RESULTS OF DESIGN, OPTIMIZATION, AND OFF-DESIGN AND DISCUSSION

The design, optimization, and off-design analysis results are presented and discussed in Sections 4.1, 4.2, and 4.3, respectively. Throughout the discussion, the results of the present study are compared with published simulation results for other sCO_2 cycles implemented in various technologies, particularly nuclear reactors and concentrated solar power technologies.

4.1 | Design analysis results

Parametric analyses on the effects of the pressure ratio, TIT, CIT, and compressor outlet pressure on the thermal and exergy efficiencies, $c_{p,\text{total}}$, and LCOE are introduced in this section for each investigated cycle.

4.1.1 | Pressure ratio effect

The thermal efficiency of each cycle increases with the increase of the pressure ratio (r_c) up to an optimum value of r_c, which is 4.33 for DRC and ICC, 3.33 for the PIC, and 3.67 for the RHC (see Figure 5A). Up to the optimum r_c, the thermal efficiency is improved by 5.58%, 7.73%, 26.70%, and 2.67% in the DRC, ICC, PIC, and RHC, respectively. This means that the PIC is the most sensitive cycle for the variation of r_c and has the minimum optimal r_c. In contrast (as shown in Figure 5B), the exergy efficiency decreases over the range of r_c except for

TABLE 2 Validation of the energy model for each configuration (at design conditions)

Parameter	DRC	ICC	PIC	RHC
Reference	[50]	[57]	[65]	[59]
P_{net} (MW)	10	50	126	903
$T_{t,i}$ (°C)	700	600	550	1150
$T_{c,i}$ (°C)	45	45	32	33
$P_{c,o}$ (°C)	25	25	20	30
r_c	3.1	3.3	4.7	3.9
η_t (%)	93	93	90	89
η_c (%)	89	89	89	85
HTR effectiveness (%)	93	91	86	90
LTR effectiveness (%)	91	88	86	90
Thermal efficiency (%), [Ref.]	47.60	37.60	42.00	48.75
Thermal efficiency (%), [Calculated]	47.26	37.22	41.23	48.34
Absolute relative error, ARE (%)*	0.71	1.01	1.83	0.84

Note: ARE = 100 × |Ref. − Calculated|/Ref.

Abbreviations: DRC, dual recuperator cycle; ICC, intercooling cycle; PIC, partial intercooling cycle; RHC, reheating cycle.

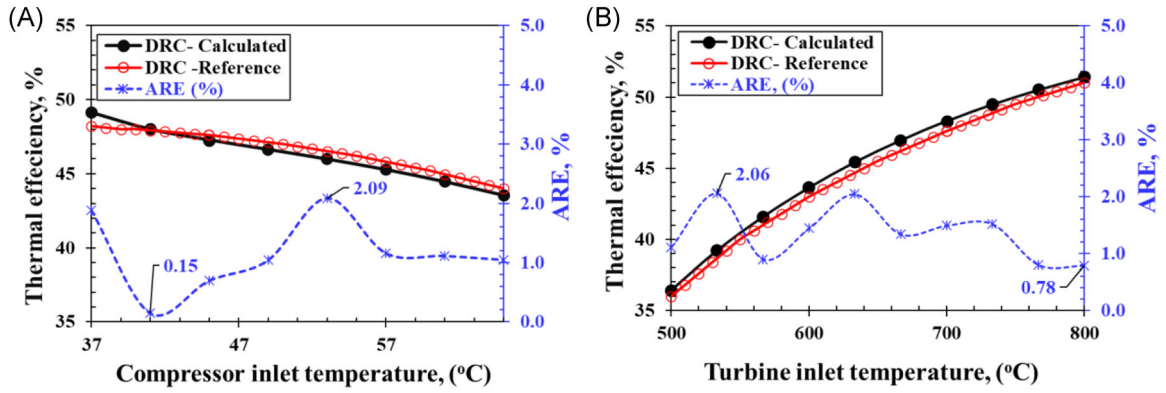

FIGURE 4 Thermal efficiency variation of the dual recuperator cycle (DRC) with (A) inlet temperature of compressor, and (B) inlet temperature of the turbine based on the off-design analysis results of this study (calculated) compared to Dyreby et al[51]

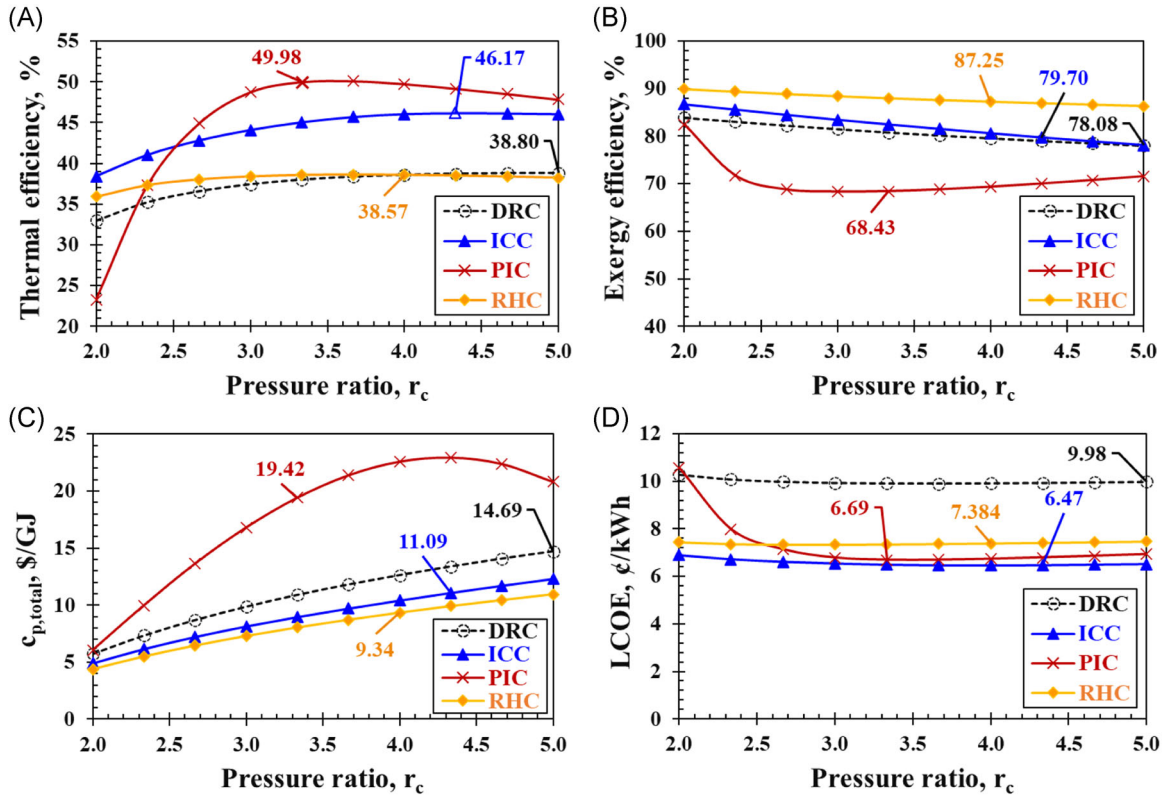

FIGURE 5 Relationship between the pressure ratio and (A) thermal efficiency, (B) exergy efficiency, (C) total product unit cost, and (D) LCOE of each cycle. At TIT = 750°C, CIT = 50°C, and $P_{c,o}$ = 20 MPa. CIT, compressor inlet temperature; DRC, dual recuperator cycle; ICC, intercooling cycle; LCOE, levelized cost of electricity; PIC, partial intercooling cycle; RHC, reheating cycle; TIT, turbine inlet temperature

the PIC, which decreases first up to $r_c = 2.67$ then increases at $r_c > 2.67$. However, the PIC has the lowest exergy efficiency compared to the other cycles. Also, the decrease of the exergy efficiency has the dominant effect on $c_{p,\text{total}}$, which causes its increase with r_c (Figure 5C). Although PIC has the highest thermal efficiency (49.98%) at its optimal r_c (3.33), its LCOE is higher than the ICC by 3.4% as shown in Figure 5D. This points out that the addition of an extra compressor for the PIC has a negative effect on the LCOE more than the improvement achieved in the thermal efficiency. To avoid repetition, a further discussion that explains the technical reasons for the behavior of thermal and exergy efficiencies with the variation of r_c can be found in Sleiti and Al-Ammari.[23] This is applied also for Sections 4.1.2 and 4.1.3. Therefore, particular focus will be given to the exergoeconomic and LCOE results.

For comparison, the optimal efficiencies of the PIC and ICC cycles (49.98% and 46.17%) are competitive for that of recompression sCO_2 power cycle driven by the nuclear reactor, which was 48.76% (without intercooling) and 50.05% (with intercooling) as reported by Ma et al.[73] However, reported results were obtained at a reactor temperature of 850°C, high pressure of 20 MPa, and CIT of 35°C. This means that the DOC-based PIC and ICC cycles achieve competitive performance at moderate TIT and may have even higher efficiencies than the recompression cycle at low compressor inlet temperatures as discussed in Section 4.1.3. Furthermore, as shown in Figure 5D, it is found that the LCOE of the DRC is the highest (9.98 ¢/kWh as average), which is higher than of other cycles by 54.25% for ICC, 49.20% for PIC, and 33.70% for RHC. However, the LCOE of the DOC-based DRC cycle is lower than those driven by concentrated solar power (e.g., 17.6 ¢/kWh,[74] at TIT = 700°C and CIT = 55°C) and comparable for coal-based sCO_2 power cycles (e.g., 9.0 ¢/kWh,[75] at TIT = 620°C and CIT = 32°C).

4.1.2 | Effect of turbine inlet temperature

Although the Allam cycle has high efficiency (58%), it still has disadvantages at the technical level as it works at TIT of 1150°C and high pressure of 30 MPa, which dictates unconventional designs for its components.[76] In particular, the turbine must be cooled and the recuperator has to withstand high temperatures (up to 750°C). Therefore, as a new approach, it is recommended to develop DOC-sCO_2 power cycles to operate at TIT within the range of 550–750°C.[29,47] Thus, in this section, the economic performance of the investigated cycles is presented within that range, as shown in Figure 6. As the TIT increases from 550 to 750°C, the thermal efficiency is increased by 4.31%, 2.19%, 7.90%, and 6.90% in DRC, ICC, PIC, and RHC, respectively (Figure 6A). This implies that the ICC is the least sensitive cycle to the TIT, which makes it a preferred configuration for other types of energy sources, such as nuclear reactor,[65] solar power, and waste heat energy.[62] Unlike PIC and RHC, the exergy efficiency of ICC increases by 2.50% with the increase of the TIT as shown in Figure 6B. However, the RHC has the highest exergy efficiency (87.50%) at TIT higher than 640°C. Consequently, RHC has the minimum $c_{p,total}$ (8.88 $/GJ) as shown in Figure 6C. Moreover, the exergy efficiency of the present cycles is about two times higher than that of coal-fired Allam cycle (40.20%) reported by Jing Luo[77] due to: (1) the extremely high TIT (1150°C), which increases the destruction rate through cycle components, and

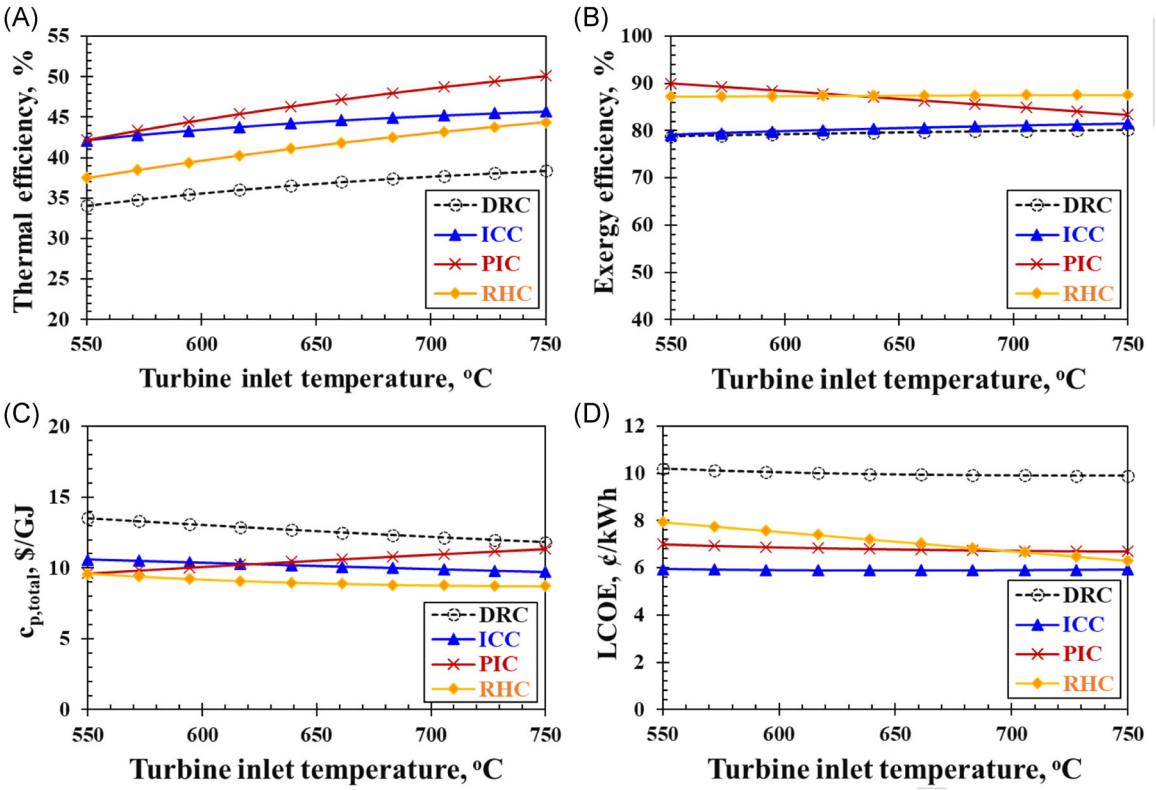

FIGURE 6 Relationship between the turbine inlet temperature and (A) thermal efficiency, (B) exergy efficiency, (C) total product unit cost, and (D) LCOE of each cycle. At $r_c = 3.67$, CIT = 50°C and $P_{c,o} = 20$ MPa. CIT, compressor inlet temperature; DRC, dual recuperator cycle; ICC, intercooling cycle; LCOE, levelized cost of electricity; PIC, partial intercooling cycle; RHC, reheating cycle

(2) numerous components of the coal-fired Allam cycle are not needed for the presented in this study DOC-based cycles such as gasification unit and syngas coolers.

Economically, as shown in Figure 6D, the LCOE of the present cycles slightly decreases with the increase of the TIT except for the RHC as its performance is significantly affected by this parameter. The stability of the LCOE with the increase of the TIT can be explained as higher TIT yield higher thermal efficiency as well as higher costs for the turbine and recuperators materials. But, for the RHC, the efficiency enhancement was more dominant than the increase of the materials cost. However, ICC still has lower LCOE (5.93 ¢/kWh) than DRC (by 41%), PIC (11%), and RHC (17%). Also, LCOE of ICC cycle in this study is less than one-half the LCOE of a recompression CO_2 cycle (5.93 ¢/kWh) that works at TIT of 750°C, CIT of 50°C, $P_{c,o}$ of 20 MPa, and r_c of 2.6 as reported by Noaman et al.[64]

4.1.3 | Effect of compressor inlet temperature

The CIT depends on the cooling method performed in the plant such that temperatures less than 35°C are only achievable by wet cooling techniques while dry cooling provides CIT higher than 45°C.[78] However, the economic aspects of each wet and dry cooling approach are considerably different; thus, an economic comparison must be conducted to decide the most feasible and efficient method.[47] For the present cycles, the effects of the CIT on the thermal efficiency, exergy efficiency, $c_{p,total}$, and LCOE of each cycle are presented in Figure 7. For all cycles, the thermal efficiency is improved only by 2% (average) as the *CIT* decreases from 50 to 33°C. Also, LCOEs at *CIT* of 33°C (wet cooling) are 9.51, 5.72, 7.27, and 7.07 ¢/kWh for DRC, ICC, PIC, and RHC, respectively. These LCOEs are lower than at dry cooling conditions (CIT of 50°C) by 4.0%, 3.5%, 2.6%, and 3.9%, respectively. This implies that these DOC-based cycles are less sensitive for the cooling method than the solar-based recompression cycle as its efficiency in dry cooling is about 6% lower than in wet cooling conditions. Therefore, the present cycles are economically feasible even in harsh environmental conditions at which dry cooling methods are more practical than wet cooling methods.

4.1.4 | Effect of compressor outlet pressure

The aforementioned results were presented at constant high pressure ($P_{c,o}$) of 20 MPa. However, $P_{c,o}$ has a key

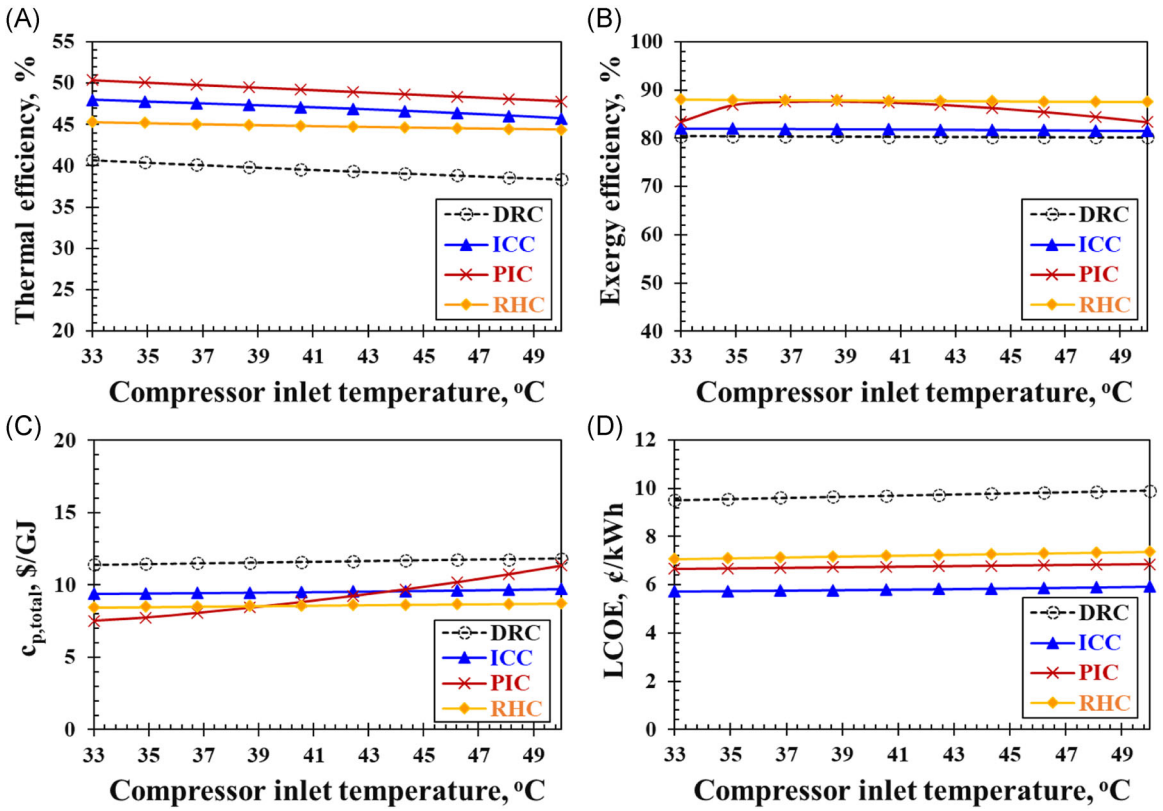

FIGURE 7 Relationship between the compressor inlet temperature and (A) thermal efficiency, (B) exergy efficiency, (C) total product unit cost, and (D) LCOE of each cycle. At $r_c = 3.67$, TIT = 750°C and $P_{c,o} = 20$ MPa. DRC, dual recuperator cycle; ICC, intercooling cycle; LCOE, levelized cost of electricity; PIC, partial intercooling cycle; RHC, reheating cycle; TIT, turbine inlet temperature

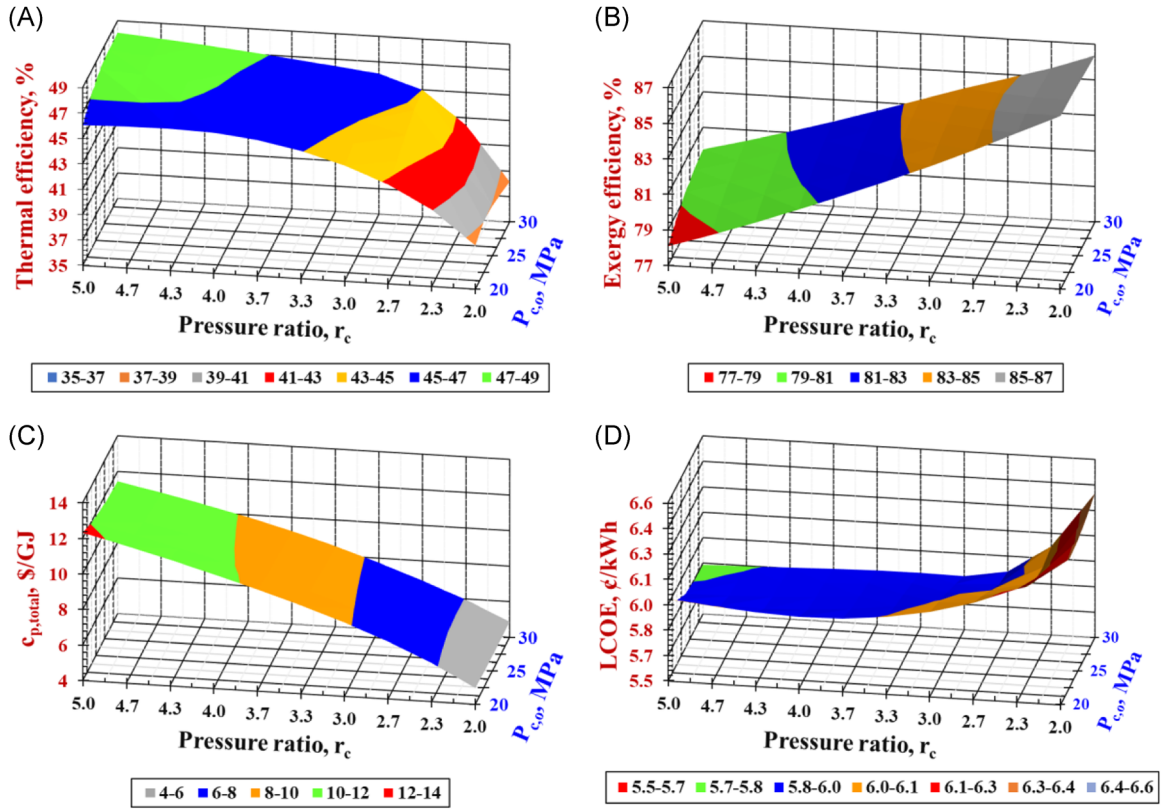

FIGURE 8 Effect of the compressor outlet pressure ($P_{c,o}$), and pressure ratio on the (A) thermal efficiency, (B) exergy efficiency, (C) total product unit cost, and (D) *LCOE* of the ICC. At TIT = 750°C and CIT = 50°C. CIT, compressor inlet temperature; LCOE, levelized cost of electricity; TIT, turbine inlet temperature

role in the performance of the present cycles and affects the value of the optimized pressure ratio. As the ICC shows superior economic performance compared to the other cycles with comparable efficiencies for the PIC, it was selected for further analysis for the high-pressure effect. Therefore, the 4E performance indicators for the ICC were simulated over the range of r_c (2–5) at different high pressures (20–30 MPa) as shown in Figure 8. Within this range, the thermal efficiency is increased from 38.44% (at $P_{c,o} = 0$ MPa and $r_c = 2$) to 46.07% (at $P_{c,o} = 30$ MPa and $r_c = 3$) at the same low-side pressure. Also, it is increased to 48.05% (at $P_{c,o} = 30$ MPa and $r_c = 5$) but with lower pressures at the low-pressure side. Furthermore, it is found that the optimum r_c for the thermal efficiency differs from the optimum one for the LCOE at $P_{c,o}$ less than 25 MPa. For instance, at $P_{c,o}$ of 22.5 MPa, the optimum r_c for maximum efficiency is 4.67 while it is 4.00 for minimum LCOE. Moreover, these results are subject to change if the CIT is changed. Therefore, to optimize the 4E performance indicators, an optimization analysis is necessary, which is conducted and presented in the next section.

4.2 | Optimization results

For sCO_2 power cycle optimization analysis, the genetic algorithm (GA) approach is recommended as it was less sensitive for the initial guess values, which yield robust results compared to other optimization techniques.[35,44,79] Thus, the GA optimization tool is used in EES to do single- and multiobjective optimization. The high-pressure ($P_{c,o}$), low-pressure ($P_{c,i}$), and the CIT are the major operating conditions that affect the amount of the recycled CO_2 flow rate, fuel flow rate, size of the recuperators and precoolers, and the size of the turbomachinery components (turbines and compressors). Therefore, these parameters are considered as decision variables to be optimized within their practical ranges as:

$$20 \le P_{c,o}\text{MPa} \le 30,$$

$$4 \le P_{c,i}\text{MPa} \le 15,$$

$$550 \le \text{TIT°C} \le 750,$$

$$30 \le \text{CIT°C} \le 50.$$

TABLE 3 Optimization results

Cycle	Optimization function	Decision variables				Optimized results			
		$P_{c,o}$ (MPa)	$P_{c,i}$ (MPa)	TIT (°C)	CIT (°C)	ηth (%)	$\varepsilon_{overall}$ (%)	$c_{p,total}$ (S/GJ)	LCOE (¢/kWh)
DRC	*Max.* η_{th}	30	8	748	33	47.88	81.12	10.20	8.47
	Max. $\varepsilon_{overall}$	20	8	745	35	40.97	82.99	7.31	9.12
	Min. $c_{p,total}$	20	8	745	33	41.85	82.94	7.14	8.97
	Min. LCOE	30	8	581	33	46.61	79.96	10.90	8.28
	Max. MOF	30	8	747	33	47.97	81.11	10.17	8.46
ICC	*Max.* η_{th}	29	8	739	33	51.95	83.06	5.40	5.73
	Max. $\varepsilon_{overall}$	20	8	750	34	46.88	85.49	5.66	5.61
	Min. $c_{p,total}$	20	8	739	33	47.04	85.54	5.62	6.01
	Min. LCOE	28	8	563	33	49.74	81.55	5.30	5.53
	Max. MOF	30	8	744	33	52.08	83.04	5.39	5.65
PIC	*Max.* η_{th}	20	5	749	35	51.97	86.49	10.53	7.88
	Max. $\varepsilon_{overall}$	28	8	740	34	49.82	88.76	8.53	8.02
	Min. $c_{p,total}$	20	3	550	33	39.63	68.12	11.22	9.02
	Min. LCOE	20	3	750	33	52.00	59.60	9.68	7.13
	Max. MOF	30	8	748	33	49.20	73.13	10.33	7.46
RHC	*Max.* η_{th}	29	8	715	33	49.01	89.48	7.29	8.01
	Max. $\varepsilon_{overall}$	20	8	550	33	44.87	90.28	5.50	7.86
	Min. $c_{p,total}$	26	3	610	35	34.93	84.61	5.09	7.96
	Min. LCOE	27	8	550	33	47.18	89.71	7.31	7.90
	Max. MOF	30	8	616	33	48.62	89.50	7.55	8.04

Abbreviations: DRC, dual recuperator cycle; ICC, intercooling cycle; LCOE, levelized cost of electricity; PIC, partial intercooling cycle; RHC, reheating cycle.

Based on the optimization methodology shown in the Supporting Information Material (Figure S1), four objective functions were selected, including maximizing the thermal efficiency (η_{th}), maximizing the exergy efficiency ($\varepsilon_{overall}$), minimizing $c_{p,total}$, and minimizing the LCOE as single optimization functions (SOFs). Also, for multi-objective optimization, a multiobjective function (MOF) is defined as follows:

$$\begin{aligned} \text{Max.MOF} = {} & w_1 \times \eta_{th} + w_2 \times \varepsilon_{overall} \\ & + w_3 \times \left(1 - \frac{c_{p,total}}{c_{unit,f}}\right) \\ & + w_4 \times \left(1 - \frac{LCOE}{C_{fuel}}\right), \end{aligned} \tag{29}$$

where $c_{unit,f}$ and C_{fuel} are the unit fuel cost (26.64 $/GJ) and fuel cost (12 ¢/kWh), respectively. The results of the SOF and MOF for the present cycles are presented in Table 3.

Figure 9 compares the results obtained for the 4E performance indicators by the single-bojective and multi-objective optimization fuctions. It is found that Min. $c_{p,total}$ and Max.MOF yield decision parameters at which ICC has more efficient performance than the PIC (Figure 9A). Therefore, at optimized conditions, ICC shows superior energetic (52.08%) and economic (5.65 ¢/kWh) performances over the other cycles. However, the exergetic performance of the ICC (83.04%) is about 6% lower than that of the RHC Figure 9B. However, the energetic performance of the ICC is more dominant and yields lower $c_{p,total}$ (5.39 $/GJ) than other cycles. In comparison to the optimized efficiency (49%) for a solar-based recompression cycle that works at TIT of 650°C, CIT of 40°C, $P_{c,o}$ of 24.8 MPa, and $P_{c,i}$ of 7.8 MPa reported by Reyes-Belmonte et al.,[80] the present

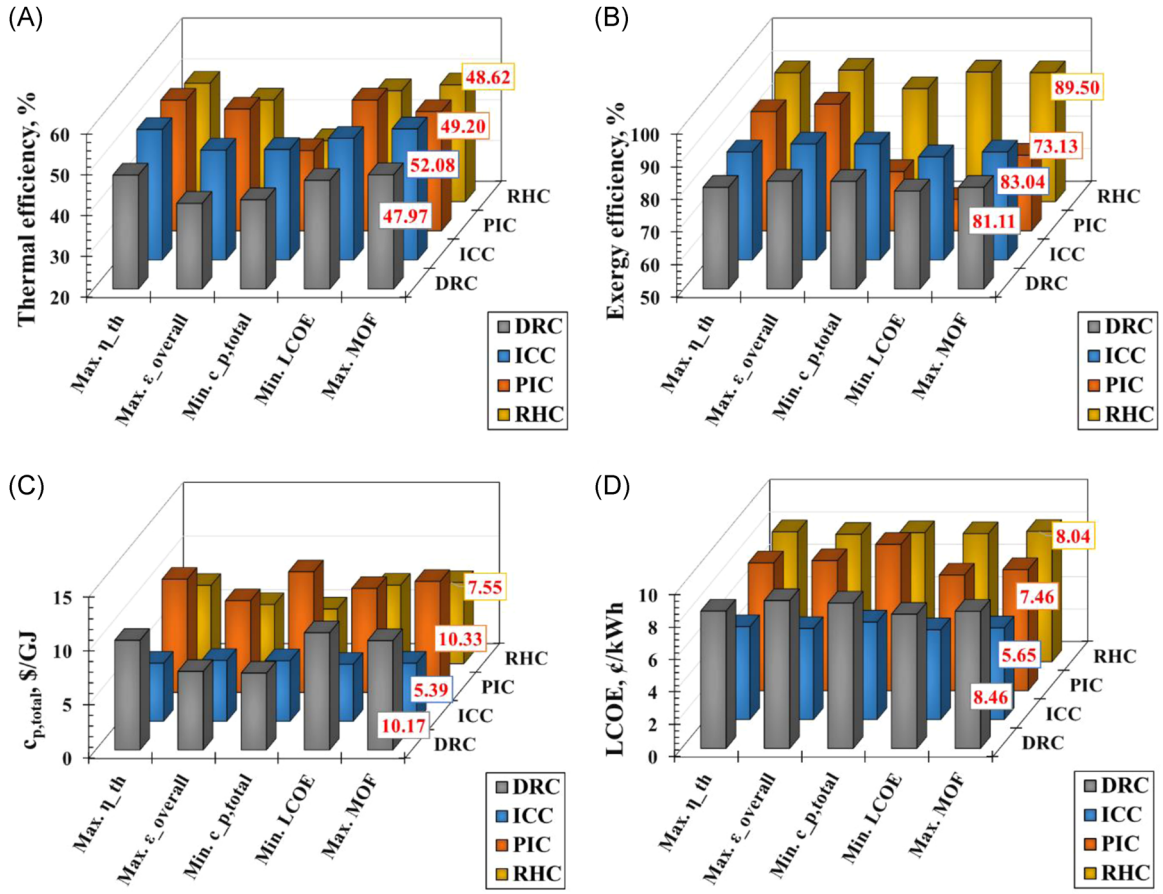

FIGURE 9 Comparison of the optimized results for each cycle by the selected optimization functions. DRC, dual recuperator cycle; ICC, intercooling cycle; LCOE, levelized cost of electricity; PIC, partial intercooling cycle; RHC, reheating cycle

ICC has an efficiency of 49.74% at TIT of 563°C, CIT of 33°C, $P_{c,o}$ of 28 MPa, and $P_{c,i}$ of 8 MPa as obtained by Min. LCOE function (Table 3).

At the optimized designed conditions, the exergy destruction of the components of each cycle is calculated from the fuel and product exergies presented in the supplementary data (Table S5) and analyzed as shown in Figure 10. Also, Table S5 shows the capital cost of each component and the total capital cost of each cycle. It is found that the oxy-combustor is responsible for the major part of exergy destruction of each cycle with a minimum share of 54% in the PIC and a maximum share of 74% in the ICC. This is explained by the chemical reactions and significant temperature difference that occurs through the combustion process. Also, the heat exchanger components (recuperators and precoolers) contribute significantly to the exergy destruction with a maximum of 43% in the PIC as it has two precoolers with a lower recycled flowrate. This reduces the heat transfer coefficient with the cooling fluid and enhances the exergy destruction share. From exergoeconomic point of view, the exergoeconomic factor of each component is calculated as follows:

$$f_k = \dot{Z}_K/(\dot{Z}_K + \dot{C}_{D,k}), \tag{30}$$

where $\dot{Z}_K$ and $\dot{C}_{D,k}$ are the cost rate of the component cost and its exergy destruction, respectively. The average exergoeconomic factor of the oxy-combustor ($f_{co} = 82.21\%$ as) is higher than that of the turbomachinery (48.98%) and heat exchanger (33.87%) components (Table S5). However, the contribution of the turbomachinery components to the exergy destruction is the least among the other components (Figure 10). Therefore, improving the design of the combustor and recuperators is essential to enhance the energy performance of the cycles.

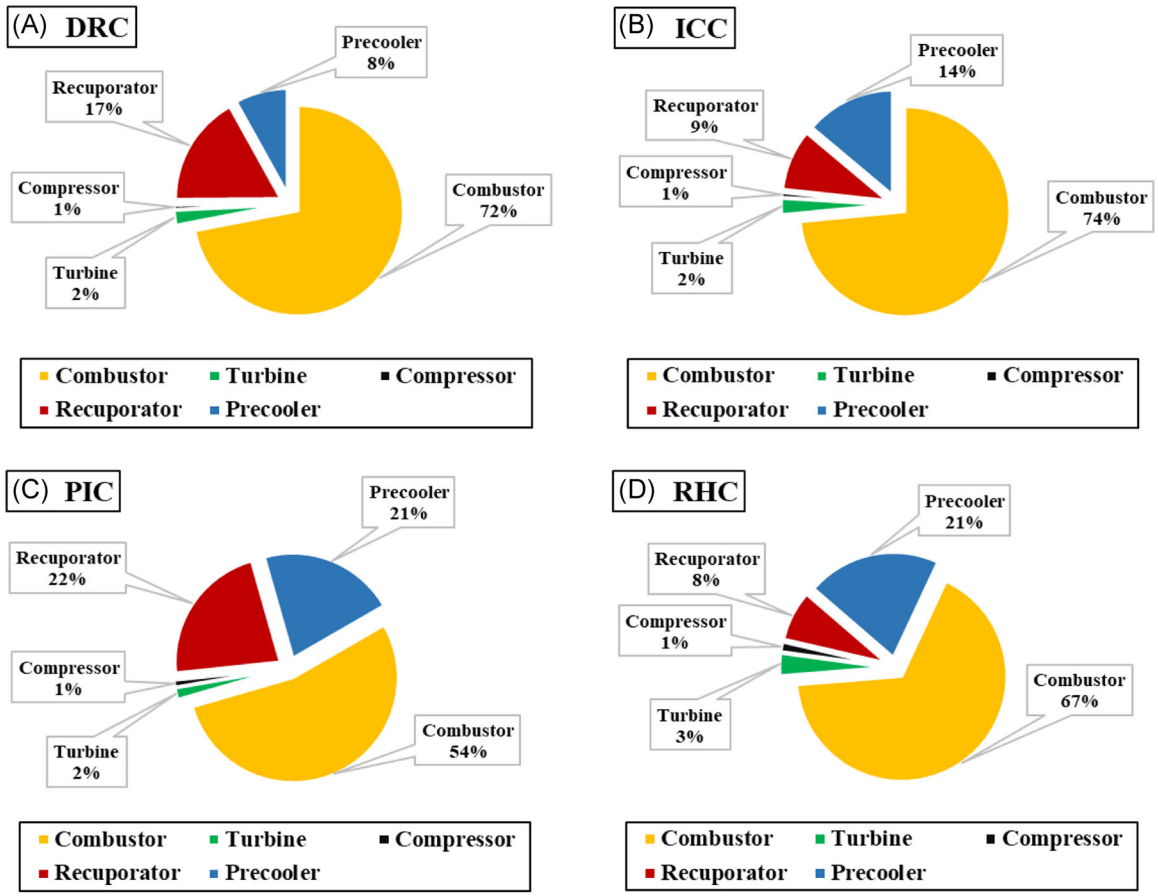

FIGURE 10 Comparison of the exergy destruction share of each component in the investigated cycles at their optimized conditions. DRC, dual recuperator cycle; ICC, intercooling cycle; PIC, partial intercooling cycle; RHC, reheating cycle

4.3 | Off-design analysis results

The above results were obtained at constant turbomachinery efficiencies (89% for compressors and 93% for turbines) and fixed output power of 50 MW. However, these parameters are varied with the variation of the CIT, TIT, and PD profiles. Therefore, using the off-design model, the performance of each cycle is simulated at off-design conditions as shown in Figure 10. First, the thermal efficiency and LCOE were calculated at fixed control variables (FCVs), which are the shaft speed (N_c) and the compressor inlet pressure ($P_{c,i}$). Then, N_c and $P_{c,i}$ were adjusted to maximize the energy efficiency and minimize the LCOE. The adjustment of the control variables by reducing $P_{c,i}$ (from 8 to 7.7 MPa) and shaft speed (from 13,000 to 10,000 rpm) as the CIT increases from 33 to 50°C. This, in turn, maintains the dense behavior of the sCO_2 and minimizes the compression power. At optimized conditions and FCVs, the thermal efficiency of ICC is higher than other cycles at CIT of 33°C (Figure 10A). But, at CIT higher than 37°C, the PIC is the most efficient cycle; however, the *LCOE* of the ICC is the minimum over the range of the CIT (Figure 10B). Furthermore, the ICC shows superior performance compared to PIC at TIT less than 700°C. Moreover, the adjustment of the control variables considerably improves the thermal efficiency of the ICC by 2.0% at dry cooling conditions (CIT > 40°C) and by 0.6% at TIT > 640°C. This improvement is comparable to that of the recompression cycle investigated by Dyreby et al.,[50] which was about 2.5% for the CIT and 1.5% for the TIT.

Figure 11 shows the energetic and economic performance of the present cycles at variable PD profiles for two typical days in Qatar (namely, September 7 for Max. PD, and February 1 for Min. PD). It is found that as the PD reduced from 50 to 21 MW (42% of the design output power), the thermal efficiency is reduced by 21.82% in DRC, 17.71% in ICC, 22.46% in PIC, and 13.60% in RHC. This implies that the RHC is the least sensitive cycle for the variation of the PD, thus its LCOE is slightly changing with the PD profile Figure 11D. However, the

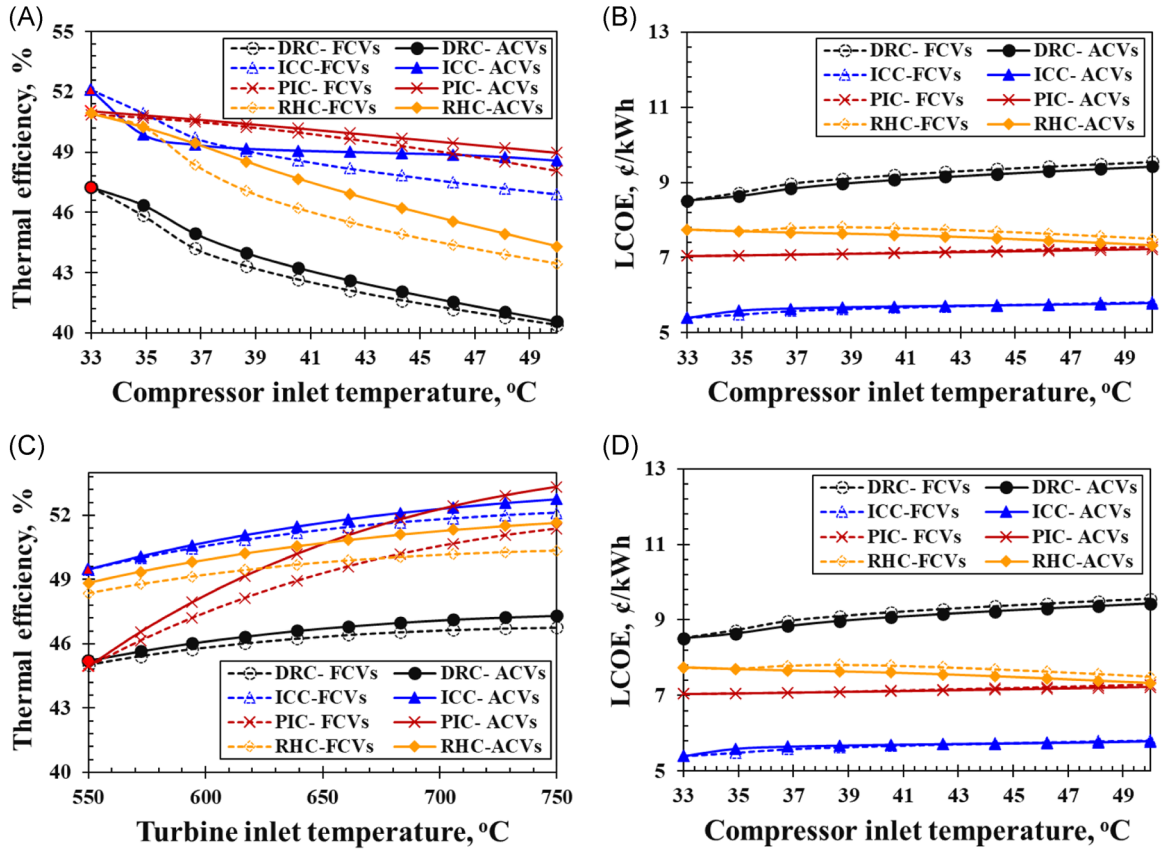

FIGURE 11 The variation of the thermal efficiency and LCOE with the compressor inlet temperature (A, B) and with turbine inlet temperature (C, D) at fixed control variables (FCVs) and adjusted control variable (ACVs) for each cycle. DRC, dual recuperator cycle; ICC, intercooling cycle; LCOE, levelized cost of electricity; PIC, partial intercooling cycle; RHC, reheating cycle

ICC still has the minimum LCOE with an average of 5.65 ¢/kWh at Max. PD, and 7.2 ¢/kWh at Min. PD (Figure 11B). In addition, the exergetic performance of the ICC is not affected by the conditions at part-load operations as shown in Figure 12. For compression, the thermal efficiency of a recompression cycle, intercooled cycle, and reheating cycle are reduced by 25.5%, 28.7%, and 21.1%, respectively, as PD reduced to 30% from the design load (10 MW) as reported by Yang et al.[81] This confirms the efficient and economic feasibility of the ICC for DOC-based sCO_2 power cycles in a comparable manner for the recompression cycle recommended for nuclear, solar, and waste energy technologies, as shown in Figure 13.

4.4 | Environmental analysis

To evaluate the CO_2 emissions of the present direct oxy-combustion cycles, the product CO_2 from the combustion process is calculated and compared to that of a conventional natural gas Brayton cycle (BC) with an energy efficiency of 32.0%. The net output power of all cycles is fixed at 50 MW. As shown in Figure 14, the PIC has the minimum CO_2 emissions (0.180 million tons/year[82]) while the DRC has the maximum CO_2 emissions (0.224 million tons/year) among the direct oxy-combustion-based cycles. These values are proportional to their fuel consumption and energy efficiencies as discussed in Section 4.1. However, the CO2 emissions from the conventional natural gas BC are 20% higher than the DRC and 51% higher than the PIC. Furthermore, the CO_2 emissions from the direct oxy-combustion processes are captured and exported as compressed gas to be used in commercial applications or sequestrated, which is not performed in the conventional Brayton cycles. Therefore, the present direct oxy-combustion cycles virtually have zero CO_2 emissions.

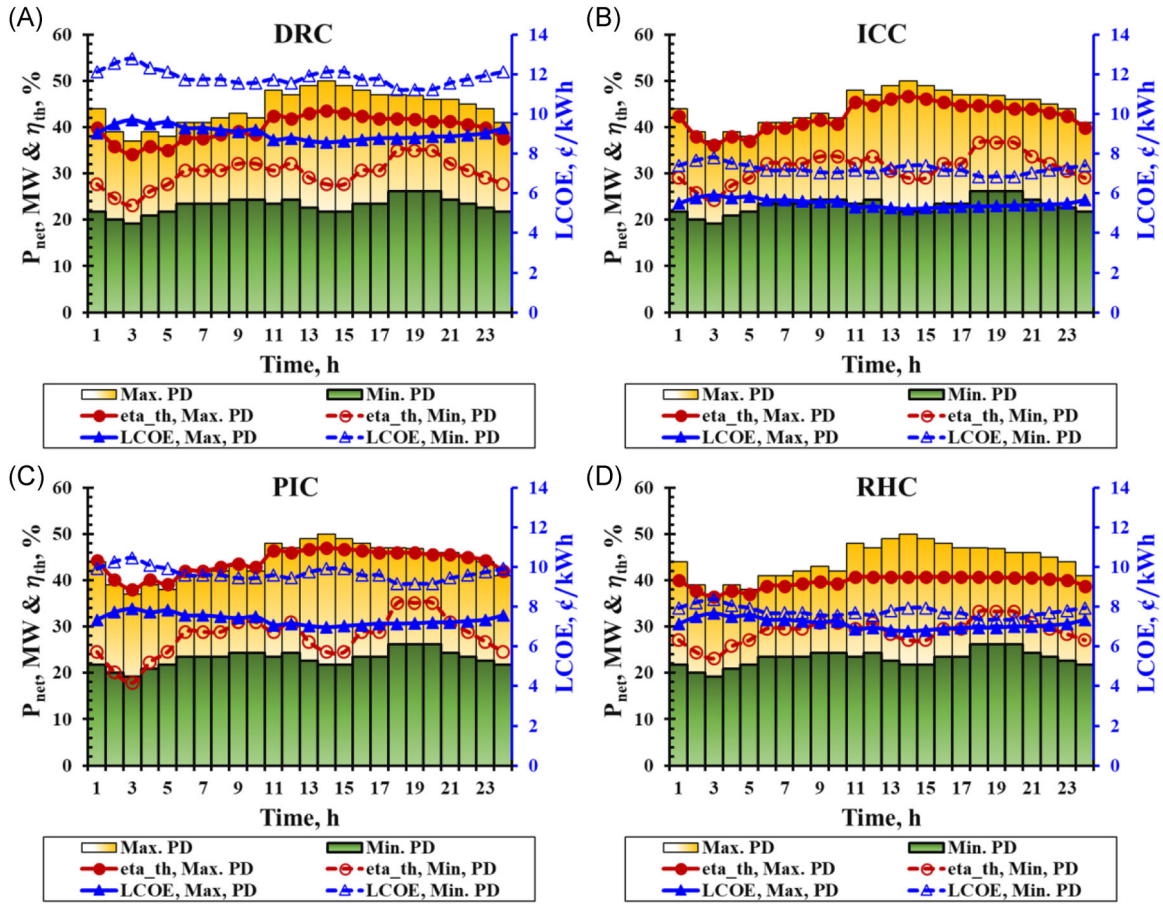

FIGURE 12 The variation of the thermal efficiency and LCOE of each cycle according to the maximum and minimum power demand (*PD*) profiles. DRC, dual recuperator cycle; ICC, intercooling cycle; LCOE, levelized cost of electricity; PIC, partial intercooling cycle; RHC, reheating cycle

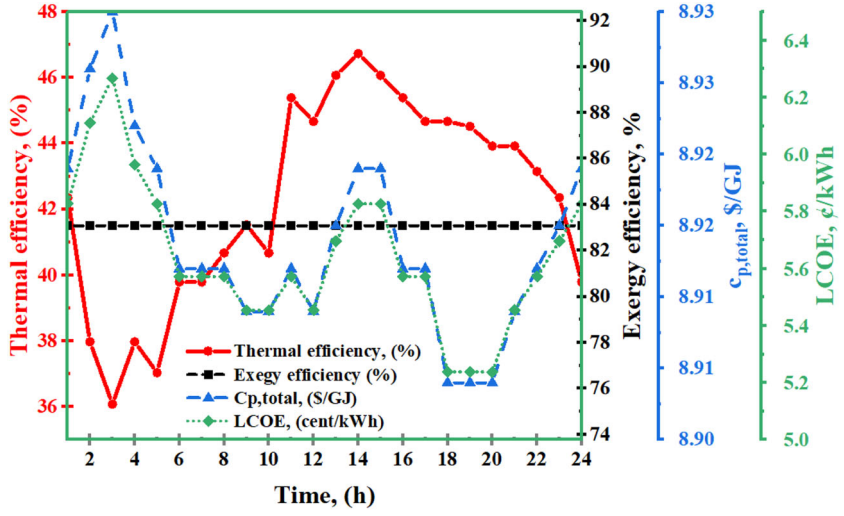

FIGURE 13 4E performance indicators of the intercooling cycle at part-load operation (for maximum power demand profile). LCOE, levelized cost of electricity

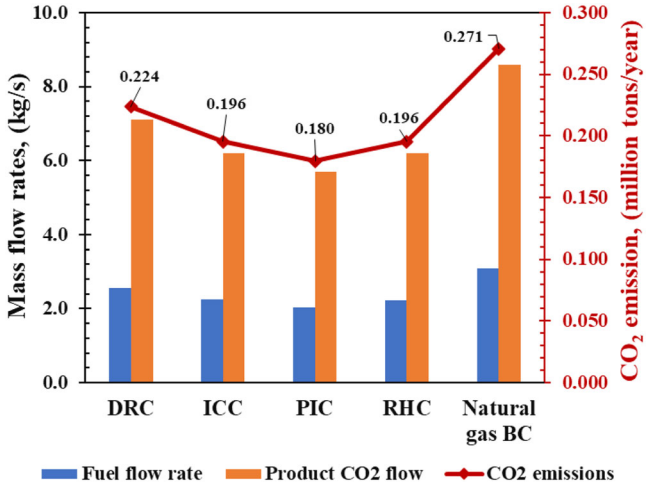

FIGURE 14 CO_2 emissions of the direct oxy-combustion-based power plants compared to the conventional natural gas Brayton-cycle-based plants

5 | CONCLUSIONS

In this study, comprehensive 4E performance analyses for four DOC-based sCO_2 power cycles at design conditions are introduced. The investigated cycles include DRC, ICC, PIC, and RHC. Then, single- and multi-objective optimization analyses were conducted for each cycle. In addition, the performance of these cycles was assessed at off-design and part-load operation conditions. The main conclusions of this study are:

(1) At design conditions ($P_{c,o} = 20$ MPa, $P_{c,o} = 5.4$ MPa, TIT = 750°C, CIT = 50°C [dry-cooling]), the PIC has the highest thermal efficiency of 47.78% compared to 38.36% for DRC, 45.71% for ICC, and 44.39% for RHC.
(2) At optimized conditions ($P_{c,o}$ =30 MPa, $P_{c,o}$ =8 MPa, TIT = 744°C, CIT = 30°C [wet-cooling]), the ICC shows superior energetic performance (52.08%) compared to 47.97% for DRC, 49.20% for PIC, and 48.62% for RHC.
(3) At off-design conditions with a PD of 40% of the design load (50 MW), the thermal efficiency is decreased by 21.82% in DRC, 17.71% in ICC, 22.46% in PIC, and 13.60% in RHC.
(4) The ICC has the minimum LCOE compared to the other cycles with 5.93 ¢/kWh at design conditions (dry-cooling), 5.65 ¢/kWh at optimized conditions (wet-cooling), and 7.2 ¢/kWh at minimum PD (21 MW).
(5) The ICC shows efficient and economic performance compared to the recompression cycle recommended for nuclear, solar, and waste energy technologies. Also, it has more practical and feasible design parameters than the Allam cycle, which requires special designs for its components as it operates at TIT higher than 1150°C.

While the present study introduces a thorough analysis for the DOC-based sCO_2 cycles at design and off-design conditions, further optimization analysis based on the detailed model of each cycle component at various control strategies is recommended for future work.

ACKNOWLEDGMENTS

The work presented in this publication was made possible by NPRP-S grant # (11S-1231-170155) from the Qatar National Research Fund (a member of the Qatar Foundation). The findings herein reflect the work, and are solely the responsibility, of the authors. Open access funding provided by the Qatar National Library

CONFLICTS OF INTEREST

The authors declare no conflicts of interest.

AUTHOR CONTRIBUTIONS

Wahib A. Al-Ammari: conceptualization, writing-original draft, investigation, software, data curation, validation, and formal analysis. **Ahmad K. Sleiti**: conceptualization, investigation, writing-original draft, review and editing, resources, formal analysis, project administration, funding acquisition, and supervision.

NOMENCLATURE

A	cross-sectional/surface area (m^2)
$c_{p,\text{total}}$	total product unit cost ($/GJ)
D	diameter (m)
$\dot{E}$	exergy rate (kW)
h	specific enthalpy (kJ/kg)
$\dot{m}$	mass flow rate (kg/s)
$\dot{n}$	molar flow rate (kmol/s)
N	shaft speed (rpm)
P	pressure (MPa)
P_{net}	net power produced by the power cycle
Q	heat transfer rate (kW)
T	temperature (°C)
$\dot{W}$	power produced (or consumed) (kW)
$\dot{W}_{c,a}$	actual power consumed by the compressor
η_{th}	thermal efficiency of the cycle (%)
ρ	fluid density (kg/m^3)
ε	exergy efficiency (%)

SUBSCRIPTS

1, 2, 3, ...	state points as shown in Figure 1
CO_2	total carbon dioxide flow
CH_4	for methane
c	for compressor

co	for combustor
cf	cold fluid
F	for fuel exergy
hf	hot fluid
H_2O	for water vapor
i	at inlet
o	at outlet
O_2	for oxygen

ORCID

Wahib A. Al-Ammari https://orcid.org/0000-0003-2923-4890
Ahmad K. Sleiti https://orcid.org/0000-0003-0947-490X

REFERENCES

1. Crespi F, Gavagnin G, Sánchez D, Martínez GS. Supercritical carbon dioxide cycles for power generation: a review. *Appl Energy*. 2017;195:152-183. doi:10.1016/j.apenergy.2017.02.048
2. Li W, Yu Z. Heat exchangers for cooling supercritical carbon dioxide and heat transfer enhancement: a review and assessment. *Energy Rep*. 2021;7:4085-4105. doi:10.1016/j.egyr.2021.06.089
3. Liu Y, Wang Y, Huang D. Supercritical CO_2 Brayton cycle: a state-of-the-art review. *Energy*. 2019;189:115900. doi:10.1016/j.energy.2019.115900
4. Srinivas T, Gupta AVSSKS, Reddy BV. Carbon dioxide emission reduction from combined cycle with partial oxidation of natural gas. *Energy Sustain. Dev*. 2009;13:33-37. doi:10.1016/j.esd.2009.01.003
5. White MT, Bianchi G, Chai L, Tassou SA, Sayma AI. Review of supercritical CO_2 technologies and systems for power generation. *Appl Therm Eng*. 2021;185:116447. doi:10.1016/j.applthermaleng.2020.116447
6. Wu P, Ma Y, Gao C, et al. A review of research and development of supercritical carbon dioxide Brayton cycle technology in nuclear engineering applications. *Nucl Eng Des*. 2020;368:110767. doi:10.1016/j.nucengdes.2020.110767
7. Du Y, Yang C, Hu C, Zhang C. Thermoeconomic analysis and inter-stage pressure ratio optimization of nuclear power supercritical CO_2 multi-stage recompression. *Int J Energy Res*. 2021;45:2367-2382. doi:10.1002/er.5932
8. Li MJ, Zhu HH, Guo JQ, Wang K, Tao WQ. The development technology and applications of supercritical CO_2 power cycle in nuclear energy, solar energy and other energy industries. *Appl Therm Eng*. 2017;126:255-275. doi:10.1016/j.applthermaleng.2017.07.173
9. Khatoon S, Ishaque S, Kim MH. Modeling and analysis of air-cooled heat exchanger integrated with supercritical carbon dioxide recompression Brayton cycle. *Energy Convers Manag*. 2021;232:113895. doi:10.1016/j.enconman.2021.113895
10. Son S, Heo JY, Kim N Il, Jamal A, Lee JI. Reduction of CO_2 emission for solar power backup by direct integration of oxy-combustion supercritical CO_2 power cycle with concentrated solar power. *Energy Convers Manag*. 2019;201:112161. doi:10.1016/j.enconman.2019.112161
11. Linares JI, Montes MJ, Cantizano A, Sánchez C. A novel supercritical CO_2 recompression Brayton power cycle for power tower concentrating solar plants. *Appl Energy*. 2020;263:114644. doi:10.1016/j.apenergy.2020.114644
12. Mohammed RH, Alsagri AS, Wang X. Performance improvement of supercritical carbon dioxide power cycles through its integration with bottoming heat recovery cycles and advanced heat exchanger design: a review. *Int J Energy Res*. 2020;44:7108-7135. doi:10.1002/er.5319
13. Abbasi HR, Yavarinasab A, Roohbakhsh S. Waste heat management of direct carbon fuel cell with advanced supercritical carbon dioxide power cycle—a thermodynamic-electrochemical modeling approach. *J CO_2 Util*. 2021;51:101630. doi:10.1016/j.jcou.2021.101630
14. Marchionni M, Bianchi G, Tassou SA. Review of supercritical carbon dioxide (sCO2) technologies for high-grade waste heat to power conversion. *SN Appl Sci*. 2020;2:1-13. doi:10.1007/s42452-020-2116-6
15. Biondi M, Giovannelli A, Di Lorenzo G, Salvini C. Techno-economic analysis of a sCO_2 power plant for waste heat recovery in steel industry. *Energy Reports*. 2020;6:298-304. doi:10.1016/j.egyr.2020.11.147
16. Allam RJ, Palmer MR, Brown GW, et al. High efficiency and low cost of electricity generation from fossil fuels while eliminating atmospheric emissions, including carbon dioxide. *Energy Procedia*. 2013;37:1135-1149. doi:10.1016/j.egypro.2013.05.211
17. Yu A, Su W, Lin X, Zhou N. Recent trends of supercritical CO_2 Brayton cycle: bibliometric analysis and research review. *Nucl Eng Technol*. 2021;53:699-714. doi:10.1016/j.net.2020.08.005
18. Neises T, Turchi C. Supercritical carbon dioxide power cycle design and configuration optimization to minimize levelized cost of energy of molten salt power towers operating at 650°C. *Sol Energy*. 2019;181:27-36. doi:10.1016/j.solener.2019.01.078
19. Li B, Wang S, Qiao J, Wang B, Song L. Thermodynamic analysis and optimization of a dual-pressure Allam cycle integrated with the regasification of liquefied natural gas. *Energy Convers Manage*. 2021;246:114660. doi:10.1016/j.enconman.2021.114660
20. Saeed M, Kim MH. Analysis of a recompression supercritical carbon dioxide power cycle with an integrated turbine design/optimization algorithm. *Energy*. 2018;165:93-111. doi:10.1016/j.energy.2018.09.058
21. Khatoon S, Kim MH. Performance analysis of carbon dioxide based combined power cycle for concentrating solar power. *Energy Convers. Manag*. 2020;205:112416. doi:10.1016/j.enconman.2019.112416
22. Milani D, Luu MT, McNaughton R, Abbas A. Optimizing an advanced hybrid of solar-assisted supercritical CO_2 Brayton cycle: a vital transition for low-carbon power generation industry. *Energy Convers Manag*. 2017;148:1317-1331. doi:10.1016/j.enconman.2017.06.017
23. Sleiti AK, Al-Ammari WA. Energy and exergy analyses of novel supercritical CO_2 Brayton cycles driven by direct oxy-fuel combustor. *Fuel*. 2021;294:120557. doi:10.1016/j.fuel.2021.120557
24. Jericha H, Sanz W, Göttlich E. Design concept for large output Graz cycle gas turbines. *J Eng Gas Turbines Power*. 2008;130:1-10. doi:10.1115/1.2747260

25. Zhao Y, Chi J, Zhang S, Xiao Y. Thermodynamic study of an improved MATIANT cycle with stream split and recompression. *Appl Therm Eng*. 2017;125:452-469. doi:10.1016/j.applthermaleng.2017.05.023
26. Bolland O, Mathieu P. Comparison of two CO_2 removal options in combined cycle power plants. *Energy Convers Manag*. 1998;39:1653-1663. doi:10.1016/s0196-8904(98)00078-8
27. Fernandes D, Wang S, Xu Q, Chen D. Dynamic simulations of the allam cycle power plant integrated with an air separation unit. *Int J Chem Eng*. 2019;2019:325-340. doi:10.1155/2019/6035856
28. Scaccabarozzi R, Gatti M, Martelli E. Thermodynamic analysis and numerical optimization of the NET Power oxy-combustion cycle. *Appl Energy*. 2016;178:505-526. doi:10.1016/j.apenergy.2016.06.060
29. Sleiti AK, Al-ammari W, Ahmed S, Kapat J. Direct-fired oxy-combustion supercritical-CO_2 power cycle with novel preheating configurations—thermodynamic and exergoeconomic analyses. *Energy*. 2021;226:120441. doi:10.1016/j.energy.2021.120441
30. Liu Z, Li Z, Zhang Y, Zhang Y, Zhao B. Thermodynamic analysis of using chemical-looping combustion in Allam-Z cycle instead of common combustion. *Energy Convers Manag*. 2022;254:115229. doi:10.1016/j.enconman.2022.115229
31. Xin T, Xu C, Liu Y, Yang Y. Thermodynamic analysis and economic evaluation of a novel coal-based zero emission polygeneration system using solar gasification. *Appl Therm Eng*. 2022;201:117814. doi:10.1016/j.applthermaleng.2021.117814
32. Xu C, Liu Y, Zhang Q, et al. Thermodynamic analysis of a novel biomass polygeneration system for ammonia synthesis and power generation using Allam power cycle. *Energy Convers Manag*. 2021;247:114746. doi:10.1016/j.enconman.2021.114746
33. Byun M, Lim D, Lee B, et al. Economically feasible decarbonization of the Haber-Bosch process through supercritical CO_2 Allam cycle integration. *Appl Energy*. 2022;307:118183. doi:10.1016/j.apenergy.2021.118183
34. Rogalev A, Grigoriev E, Kindra V, Rogalev N. Thermodynamic optimization and equipment development for a high efficient fossil fuel power plant with zero emissions. *J Clean Prod*. 2019;236:117592. doi:10.1016/j.jclepro.2019.07.067
35. Alharbi S, Elsayed ML, Chow LC. Exergoeconomic analysis and optimization of an integrated system of supercritical CO_2 Brayton cycle and multi-effect desalination. *Energy*. 2020;197:117225. doi:10.1016/j.energy.2020.117225
36. Wang K, He YL. Thermodynamic analysis and optimization of a molten salt solar power tower integrated with a recompression supercritical CO_2 Brayton cycle based on integrated modeling. *Energy Convers Manag*. 2017;135:336-350. doi:10.1016/j.enconman.2016.12.085
37. Sun L, Wang D, Xie Y. Energy, exergy and exergoeconomic analysis of two supercritical CO_2 cycles for waste heat recovery of gas turbine. *Appl Therm Eng*. 2021;196:117337. doi:10.1016/j.applthermaleng.2021.117337
38. Zhang F, Liao G, E J, Chen J, Leng E, Sundén E. Thermodynamic and exergoeconomic analysis of a novel CO_2 based combined cooling, heating and power system. *Energy Convers Manag*. 2020;222:113251. doi:10.1016/j.enconman.2020.113251
39. Mohammadi K, Ellingwood K, Powell K. Novel hybrid solar tower-gas turbine combined power cycles using supercritical carbon dioxide bottoming cycles. *Appl Therm Eng*. 2020;178:115588. doi:10.1016/j.applthermaleng.2020.115588
40. Elsayed ML, Alharbi S, Chow LC. Utilization of waste heat from a commercial GT for freshwater production, cooling and additional power: exergoeconomic analysis and optimization. *Desalination*. 2021;513:115127. doi:10.1016/j.desal.2021.115127
41. Abid M, Khan MS, Ratlamwala TAH. Comparative energy, exergy and exergo-economic analysis of solar driven supercritical carbon dioxide power and hydrogen generation cycle. *Int J Hydrogen Energy*. 2020;45:5653-5667. doi:10.1016/j.ijhydene.2019.06.103
42. Yu A, Su W, Lin X, Zhou N, Zhao L. Thermodynamic analysis on the combination of supercritical carbon dioxide power cycle and transcritical carbon dioxide refrigeration cycle for the waste heat recovery of shipboard. *Energy Convers Manag*. 2020;221:113214. doi:10.1016/j.enconman.2020.113214
43. Cao Y, Habibi H, Zoghi M, Raise A. Waste heat recovery of a combined regenerative gas turbine—recompression supercritical CO_2 Brayton cycle driven by a hybrid solar-biomass heat source for multi-generation purpose: 4E analysis and parametric study. *Energy*. 2021;236:121432. doi:10.1016/j.energy.2021.121432
44. Sleiti AK, Al-Ammari WA, Al-Khawaja M. Integrated novel solar distillation and solar single-effect absorption systems. *Desalination*. 2021;507:115032. doi:10.1016/j.desal.2021.115032
45. Thanganadar D, Fornarelli F, Camporeale S, Asfand F, Gillard J, Patchigolla K. Thermo-economic analysis, optimisation and systematic integration of supercritical carbon dioxide cycle with sensible heat thermal energy storage for CSP application. *Energy*. 2021;238:121755. doi:10.1016/j.energy.2021.121755
46. Crespi F, Thermo-economic assessment of supercritical CO_2 power cycles for concentrated solar power plants. 2019.
47. Sleiti AK, Al-Ammari WA, Vesely L, Kapat JS. Thermo-economic and optimization analyses of direct oxy-combustion supercritical carbon dioxide power cycles with dry and wet cooling. *Energy Convers Manag*. 2021;245:114607. doi:10.1016/j.enconman.2021.114607
48. Sleiti AK, Al-Ammari WA, Aboueata KM. Flare gas-to-power by direct intercooled oxy-combustion supercritical CO_2 power cycles. *Fuel*. 2022;308:121808. doi:10.1016/j.fuel.2021.121808
49. Dyreby J, Klein S, Nellis G, Reindl D. Design considerations for supercritical carbon dioxide brayton cycles with recompression. *J Eng Gas Turbines Power*. 2014;136, doi:10.1115/1.4027936
50. Dyreby JJ, Klein SA, Nellis GF, Reindl DT. Modeling off-design and part-load performance of supercritical carbon dioxide power cycles, *Proc ASME Turbo Expo*. 2013;8:1-7. doi:10.1115/GT2013-95824
51. Dyreby JJ, Klein SA, Nellis GF, Reindl DT. Development of advanced off-design models for supercritical carbon dioxide power cycles. *Int Congr Adv Nucl Power Plants*. 2012;4(2012):2711-2718.

52. Yang J, Yang Z, Duan Y. Off-design performance of a supercritical CO2 Brayton cycle integrated with a solar power tower system. *Energy*. 2020;201:117676. doi:10.1016/j.energy.2020.117676
53. Li H, Fan G, Cao L, et al. A comprehensive investigation on the design and off-design performance of supercritical carbon dioxide power system based on the small-scale lead-cooled fast reactor. *J Clean Prod*. 2020;256:120720. doi:10.1016/j.jclepro.2020.120720
54. Tong Y, Duan L, Pang L. Off-design performance analysis of a new 300 MW supercritical CO_2 coal-fired boiler. *Energy*. 2021;216:119306. doi:10.1016/j.energy.2020.119306
55. Zaryab SA, Scaccabarozzi R, Martelli E. Advanced part-load control strategies for the Allam cycle. *Appl Therm Eng*. 2020;168:114822. doi:10.1016/j.applthermaleng.2019.114822
56. Scaccabarozzi R, Gatti M, Martelli E. Thermodynamic optimization and part-load analysis of the NET power cycle. *Energy Procedia*. 2017;114:551-560. doi:10.1016/j.egypro.2017.03.1197
57. Sleiti AK, Al-ammari WA. Off-design performance analysis of combined CSP power and direct oxy-combustion supercritical carbon dioxide cycles. *Renew Energy*. 2021;180:14-29. doi:10.1016/j.renene.2021.08.047
58. Li A, Hu M, Sun C, Li Z. Optimal CO_2 abatement pathway with induced technological progress for chinese coal-fired power industry. *Energy Sustain Dev*. 2017;36:55-63. doi:10.1016/j.esd.2016.03.009
59. Chan W, Lei X, Chang F, Li H. Thermodynamic analysis and optimization of Allam cycle with a reheating configuration. *Energy Convers Manag*. 2020;224:113382. doi:10.1016/j.enconman.2020.113382
60. Liao G, Liu L, J E, et al. Effects of technical progress on performance and application of supercritical carbon dioxide power cycle: a review. *Energy Convers Manag*. 2019;199:111986. doi:10.1016/j.enconman.2019.111986
61. Wu C, sen Wang S, Li J. Exergoeconomic analysis and optimization of a combined supercritical carbon dioxide recompression Brayton/organic flash cycle for nuclear power plants. *Energy Convers Manag*. 2018;171:936-952. doi:10.1016/j.enconman.2018.06.041
62. Thanganadar D, Asfand F, Patchigolla K. Thermal performance and economic analysis of supercritical carbon dioxide cycles in combined cycle power plant. *Appl Energy*. 2019;255:113836. doi:10.1016/j.apenergy.2019.113836
63. Tozlu A, Abuşoğlu A, Özahi E. Thermoeconomic analysis and optimization of a Re-compression supercritical CO_2 cycle using waste heat of Gaziantep Municipal Solid Waste Power Plant. *Energy*. 2018;143:168-180. doi:10.1016/j.energy.2017.10.120
64. Noaman M, Saade G, Morosuk T, Tsatsaronis G. Exergoeconomic analysis applied to supercritical CO_2 power systems. *Energy*. 2019;183:756-765. doi:10.1016/j.energy.2019.06.161
65. Luo D, Huang D. Thermodynamic and exergoeconomic investigation of various SCO_2 Brayton cycles for next generation nuclear reactors. *Energy Convers Manag*. 2020;209:112649. doi:10.1016/j.enconman.2020.112649
66. Fan G, Li H, Du Y, Zheng S, Chen K, Dai Y. Preliminary conceptual design and thermo-economic analysis of a combined cooling, heating and power system based on supercritical carbon dioxide cycle. *Energy*. 2020;203:117842. doi:10.1016/j.energy.2020.117842
67. Wright S, Scammell W. Economics. In *Fundamentals and Applications of Supercritical Carbon Dioxide (SCO_2) Based Power Cycles*. 2017:127–145. doi:10.1016/B978-0-08-100804-1.00006-2
68. Wang K, He YL, Zhu HH. Integration between supercritical CO_2 Brayton cycles and molten salt solar power towers: a review and a comprehensive comparison of different cycle layouts. *Appl Energy*. 2017;195:819-836. doi:10.1016/j.apenergy.2017.03.099
69. Zhang N, Lior N, Liu M, Han W. COOLCEP (cool clean efficient power): A novel CO_2-capturing oxy-fuel power system with LNG (liquefied natural gas) coldness. *Energy Utilization, Energy*. 2010;35:1200-1210. doi:10.1016/j.energy.2009.04.002
70. Weiland NT, Lance BW, Pidaparti SR. SCO_2 power cycle component cost correlations from DOE data spanning multiple scales and applications. *Proc ASME Turbo Expo*. 2019;9:1-18. doi:10.1115/GT2019-90493
71. Bayram İŞ, Koç M, Demand side management for peak reduction and PV integration in Qatar. Proceedings of the 2017 IEEE 14th International Conference on Networking, Sensing and Control (ICNSC 2017). 2017:251–256. doi:10.1109/ICNSC.2017.8000100
72. Touati F, Al-Hitmi MA, Chowdhury NA, Hamad JA, San Pedro Gonzales AJR. Investigation of solar PV performance under Doha weather using a customized measurement and monitoring system. *Renew Energy*. 2016;89:564-577. doi:10.1016/j.renene.2015.12.046
73. Ma Y, Liu M, Yan J, Liu J. Thermodynamic study of main compression intercooling effects on supercritical CO_2 recompression Brayton cycle. *Energy*. 2017;140:746-756. doi:10.1016/j.energy.2017.08.027
74. Ma Y, Morosuk T, Luo J, Liu M, Liu J. Superstructure design and optimization on supercritical carbon dioxide cycle for application in concentrated solar power plant. *Energy Convers Manag*. 2020;206:112290. doi:10.1016/j.enconman.2019.112290
75. Park SH, Kim JY, Yoon MK, Rhim DR, Yeom CS. Thermodynamic and economic investigation of coal-fired power plant combined with various supercritical CO_2 Brayton power cycle. *Appl Therm Eng*. 2018;130:611-623. doi:10.1016/j.applthermaleng.2017.10.145
76. Stanger R, Wall T, Spörl R, et al. Oxyfuel combustion for CO_2 capture in power plants. *Int J Greenhouse Gas Control*. 2015;40:55-125. doi:10.1016/j.ijggc.2015.06.010
77. Luo J, Emelogu O, Morosuk T, Tsatsaronis G. Exergy-based investigation of a coal-fired allam cycle. *Energy*. 2021;218:119471. doi:10.1016/j.energy.2020.119471
78. Ehsan MM, Guan Z, Gurgenci H, Klimenko A. Feasibility of dry cooling in supercritical CO_2 power cycle in concentrated solar power application: review and a case study. *Renew Sustain Energy Rev*. 2020;132:110055. doi:10.1016/j.rser.2020.110055
79. Zahedi R, Ahmadi A, Dashti R. Energy, exergy, exergoeconomic and exergoenvironmental analysis and optimization of quadruple combined solar, biogas, SRC and ORC

cycles with methane system. *Renew Sustain Energy Rev*. 2021; 150:111420. doi:10.1016/j.rser.2021.111420

80. Reyes-Belmonte MA, Sebastián A, Romero M, González-Aguilar J. Optimization of a recompression supercritical carbon dioxide cycle for an innovative central receiver solar power plant. *Energy*. 2016;112:17-27. doi:10.1016/j.energy.2016.06.013
81. Yang J, Yang Z, Duan Y. Part-load performance analysis and comparison of supercritical CO_2 Brayton cycles. *Energy Convers Manag*. 2020;214:112832. doi:10.1016/j.enconman.2020.112832
82. Sleiti AK, Al-Ammari WA, Al-Khawaja M. Review of innovative approaches of thermo-mechanical refrigeration systems using low grade heat. *Int J Energy Res*. 2020;44: 9808-9838. doi:10.1002/er.5556

SUPPORTING INFORMATION

Additional supporting information may be found in the online version of the article at the publisher's website.

How to cite this article: Al-Ammari WA, Sleiti AK. Comprehensive thermoeconomic, exergoeconomic, and optimization analyses of direct oxy-combustion supercritical CO_2 intercooled and reheated cycles under design and off-design conditions. *Energy Sci Eng*. 2022;10: 1272-1295. doi:10.1002/ese3.1101